Reduction of degenerate four-wave mixing spectra to relative populations I. Weak-field limit

Skip Williams[a] and Richard N. Zare[b]
Department of Chemistry, Stanford University, Stanford, California 94305

Larry A. Rahn[b]
Combustion Research Facility (MS 9051), Sandia National Laboratories, Livermore, California 94551

(Received 28 January 1994; accepted 7 April 1994)

Diagrammatic perturbation theory combined with a spherical tensor treatment allows the degenerate four-wave mixing (DFWM) signal resulting from an isotropic molecular sample to be decomposed into a sum of three multipole moments in the weak-field (no saturation) limit. The zeroth moment gives the relative internal-state population contribution, the first moment the orientation contribution, and the second moment the alignment contribution to the DFWM spectra. This treatment makes explicit how the magnitude of the DFWM signal depends on the polarizations of the other three beams and the collisional relaxation caused by the environment. A general expression is derived for the DFWM signal for an arbitrary geometric configuration of the beams (arbitrary phase matching geometry). Under the assumption that the rates of collisional relaxation of the population, the orientation, and the alignment are the same, simple analytic expressions are found for the most commonly used experimental configurations, which should facilitate the practical analysis of DFWM spectra.

I. INTRODUCTION

Laser-induced fluorescence (LIF) is a powerful spectroscopic technique for analyzing molecular species in experiments that range from chemical reaction dynamics to plasma physics. A common goal of these experiments is to extract accurate values for relative populations from the relative intensity distribution of the emitted light. Several authors have shown how the emitted light intensity depends on the excitation/detection geometry (polarization),[1–3] the temperature, pressure, and chemical composition of the experiment (collisional relaxation),[4–6] and the laser power employed (saturation).[7–9] In general, the population as well as the elements of the first- and second-rank multipole moments of the total angular momentum, called the orientation and the alignment, respectively, can be determined from low-pressure experiments performed under single-collision conditions. In collisionally dominated environments, however, the determination of these quantities becomes extremely difficult.

An appealing alternative approach to the study of collisionally dominated environments is the use of a nonlinear technique called degenerate four-wave mixing (DFWM).[10] DFWM uniquely provides information regarding the chemical composition, kinetics, and dynamics of environments that are inherently difficult to study because of radiant interference from the emission of excited species.[11] One of the most important features of DFWM is the large four-wave mixing enhancement exhibited when the laser frequency is tuned to a molecular one-photon resonance (this includes electronic, vibrational, and rotational transitions); this feature makes DFWM a very sensitive molecular probe. Other important features include sub-Doppler spectral resolution, excellent spatial and temporal resolution, imaging capabilities, nonintrusive detection, and remote sensing. Because of these attributes, the potential of DFWM spectroscopy to obtain chemical and dynamical information has generated much excitement. Like LIF, however, DFWM requires an understanding of polarization, collisional, and saturation effects before information can be extracted from the signal intensities.

At present, DFWM signal intensities are most commonly interpreted by applying the stationary absorber model proposed by Abrams and Lind,[10,12] which considers a nondegenerate two-level system in the presence of arbitrarily strong pump fields. This model accounts only for population contributions to the DFWM response and neglects contributions from orientation and alignment. This model's predictions have been applied with much success to relate saturated DFWM signal intensities to populations in experiments performed under collisionally dominated conditions.[11,13–16] Note, however, that signals from a single rotational branch and polarization configuration were used in these experiments. These conditions serve to minimize the error introduced from applying this model to molecular systems with degenerate magnetic sublevels.[17]

To date, attempts to formulate a complete model that includes polarization, collisional, and saturation effects have been unsuccessful. Studies that emphasize saturation effects[18–27] are limited to level degeneracies in the range of 1 to 3. Even numerical approaches[28] are computationally impractical at present for level degeneracies typical of molecular species. Many authors[20,29–39] have thus resorted to perturbative treatments (no saturation) to gain insight into the DFWM response of degenerate systems.

The aim of this paper (WZR1) is to present a theory of DFWM that can be used to interpret the spectra of molecular species. This goal is accomplished by deriving expressions via time-independent diagrammatic perturbation theory that

[a]Present address: Division of Chemistry Science and Technology (MS G755), Los Alamos National Laboratory, Los Alamos, NM 87545.
[b]Authors to whom correspondence should be addressed.

 0021-9606/94/101(2)/1072/21/$6.00

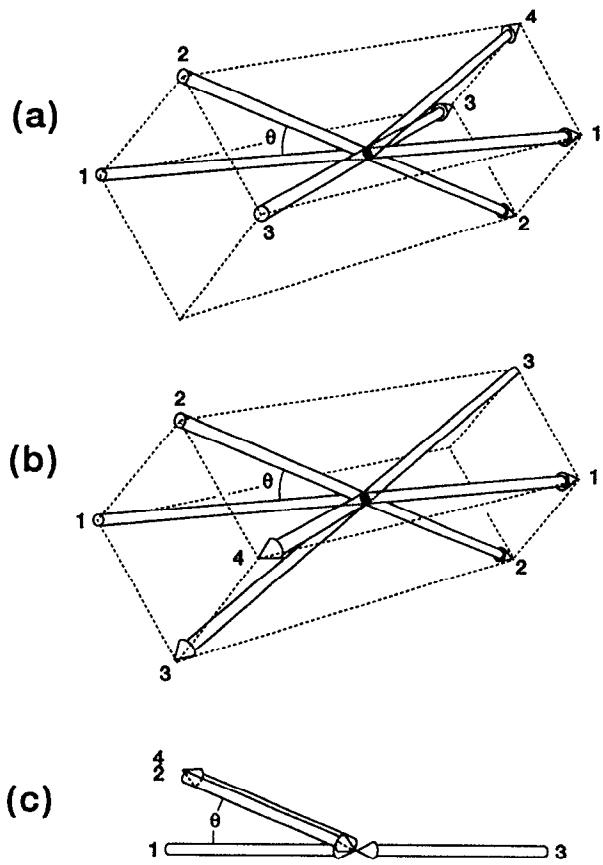

FIG. 1. Phase matching geometries: (a) Forward box, FB-DFWM; (b) Backward box, BB-DFWM; (c) Phase conjugate, PC-DFWM.

account for the DFWM polarization, collisional, and velocity effects in the weak-field limit. We consider three input fields of arbitrary polarization that interact with an isotropic sample to produce a fourth field and assume that field propagation effects can be ignored (negligible absorption). In our treatment, we assume that the DFWM process couples levels of sharp (definite) angular momentum **J** (omitting nuclear spin). Therefore, our treatment is general in that it applies to molecular species for which J is a good quantum number. The general result is specialized to apply to circularly and linearly polarized fields that interact in nearly collinear phase matching geometries in collisional environments where the multipole moments of the total angular momentum distribution relax independently (isotropic relaxation) and at the same rate. Figure 1 shows the three specific geometries we treat. In the following paper (WZR2),[17] we extend the key results presented here to interpret data taken under saturated conditions.

The remainder of this paper is organized into four sections and one appendix. In Sec. II we present expressions for the DFWM signal intensity as a function of input polarization, collisional relaxation and dephasing, and experimental geometry under the assumption that the rates of collisional relaxation of the population, the orientation, and the alignment are the same. This section is intended as a guide for the experimentalist. In Sec. III we interpret the DFWM signal intensity, as has been done for LIF, in terms of the population, the orientation, and the alignment. In Sec. IV we compare our results with those of other treatments, and in Sec. V we present conclusions of our findings. In the Appendix expressions are presented for the polarization tensor products necessary to extend this treatment to other experimental configurations.

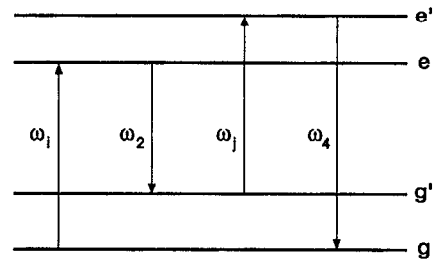

FIG. 2. Energy-level diagram for DFWM of a degenerate two-level system. In the figure $i=1$, $j=3$ or $i=3$, $j=1$.

II. DEPENDENCE OF DFWM SIGNAL INTENSITIES ON POLARIZATION, COLLISIONS, AND PHASE MATCHING GEOMETRY

A. Expressions and discussion

In four-wave mixing three incoming waves with electric fields $\mathbf{E}_1(\mathbf{r},t)$, $\mathbf{E}_2(\mathbf{r},t)$, and $\mathbf{E}_3(\mathbf{r},t)$, propagation vectors $\mathbf{k}_1$, $\mathbf{k}_2$, and $\mathbf{k}_3$, and frequencies ω_1, ω_2, and ω_3 interact through the third-order nonlinear susceptibility $\chi^{(3)}$ to generate a fourth field, $\mathbf{E}_4$, with propagation vector $\mathbf{k}_4$ and frequency ω_4. The electric fields are defined as

$$\mathbf{E}_j(\mathbf{r},t)=\tfrac{1}{2}\mathbf{E}_j e^{-i(\omega_j t-\mathbf{k}_j\mathbf{r})}+\text{c.c.}; \quad \mathbf{E}_j=\mathscr{E}_j\boldsymbol{\epsilon}_j, \tag{1}$$

where $\mathbf{E}_j$ is the vector amplitude, $\mathscr{E}_j$ is the scalar amplitude, and $\boldsymbol{\epsilon}_j$ is the normalized ($\boldsymbol{\epsilon}_j\cdot\boldsymbol{\epsilon}_j^*=1$) polarization unit vector of the electric field labeled j. The conventions for expressing the unit vectors are given in the Appendix.

For fully resonant DFWM $\omega_1=\omega_2=\omega_3=\omega_4=\omega$, and we assume that the excitation bandwidth is sufficiently narrow compared with the density of states (including Doppler broadening) of the absorbing molecules so that the interaction is exclusively between the degenerate magnetic sublevels of the two levels involved in the one-photon resonant transition. These levels are assumed to be characterized by total angular momentum **J**. Figure 2 shows a schematic energy-level diagram of the process described above. In this figure we restrict the letters g and g' to refer to two degenerate magnetic sublevels (either the same or different) of the lower level (usually the ground electronic state), and the letters e and e' refer to two degenerate magnetic sublevels (either the same or different) of the upper level (usually another electronic state). In the following discussion we adopt the standard nomenclature for the four fields involved in four-wave mixing: 1 and 3 refer to the two pump fields, 2 refers to the probe field, and 4 refers to the signal field.

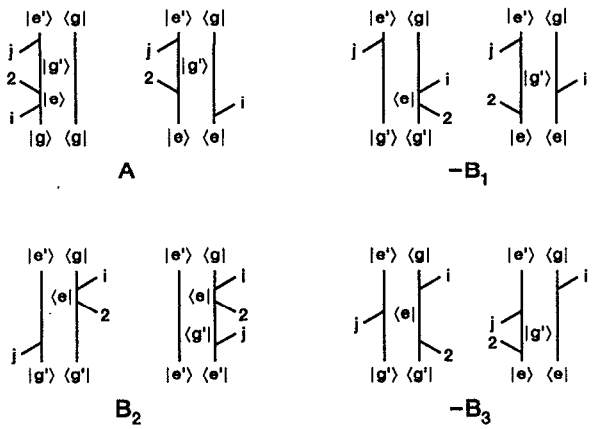

FIG. 3. Double-sided Feynman diagrams used to construct the DFWM third-order susceptibility. The first set of eight resonant contributions is formed by substituting $i=1, j=3$ and the second by $i=3, j=1$. The energy-resonant denominators of Eq. (23) associated with each set of diagrams is indicated.

The general expression for $\chi^{(3)}$ that applies here consists of 96 terms (48 for the upper level and 48 for the lower level) that completely describe the interaction of the electric fields with the molecular system.[40,41] These terms differ in the time ordering of the interaction fields and the permutations of the quantum states involved. Evaluating all of these terms is a formidable task in general; however, in a fully resonant four-wave mixing experiment, the intensity at a particular resonance in the spectrum is dominated by only 16 terms. This result is well established in the literature on resonant coherent anti-Stokes Raman spectroscopy (CARS).[33,40] These terms are represented using double-sided Feynman diagrams in Fig. 3. For fully resonant DFWM the summation over all state permutations reduces to a summation over the magnetic sublevels M_g, $M_{g'}$, M_e, and $M_{e'}$ of the two levels involved. Furthermore, if the initial magnetic sublevel distribution is isotropic, i.e., all degenerate M levels are equally populated and no phase relation exists between them, the summation is equally weighted. Taking these aspects into consideration and assuming that the collisional relaxation rates of the population, the orientation, and the alignment are the same, we write the DFWM signal intensity as

$$I_{\mathrm{DFWM}} \propto I_1 I_2 I_3 \left[N_g - \frac{(2J_g+1)}{(2J_e+1)} N_e \right]^2 [B_{ge}(J_g,J_e)]^4 \times |\mathscr{L}(\omega)|^2 |G_F^T(\boldsymbol{\epsilon}_4,\boldsymbol{\epsilon}_1,\boldsymbol{\epsilon}_3,\boldsymbol{\epsilon}_2;J_g,J_e;\omega)|^2, \tag{2}$$

where

$$\mathscr{L}(\omega) = [L_{12}^g(\omega) + L_{32}^g(\omega) + L_{12}^e(\omega) + L_{32}^e(\omega)] \tag{3}$$

is the total line shape function and

$$G_F^T(\boldsymbol{\epsilon}_4,\boldsymbol{\epsilon}_1,\boldsymbol{\epsilon}_3,\boldsymbol{\epsilon}_2;J_g,J_e;\omega) = W_{13}(\omega) G_F(\boldsymbol{\epsilon}_4,\boldsymbol{\epsilon}_1,\boldsymbol{\epsilon}_3,\boldsymbol{\epsilon}_2;J_g,J_e) + W_{31}(\omega) G_F(\boldsymbol{\epsilon}_4,\boldsymbol{\epsilon}_3,\boldsymbol{\epsilon}_1,\boldsymbol{\epsilon}_2;J_g,J_e) \tag{4}$$

is the total geometric factor. In Eq. (2) I_j is the intensity of the electric field labeled j, N_g, and N_e are the total populations of the levels g and e, respectively, in the absence of applied fields, and $B_{ge}(J_g,J_e)$ is the Einstein absorption coefficient that connects the level with total angular momentum $\mathbf{J}_g$ to the level with $\mathbf{J}_e$. In Eq. (3) the $L_{j2}^n(\omega)$ are complex line shape functions. In Eq. (4) the $G_F(\boldsymbol{\epsilon}_4,\boldsymbol{\epsilon}_i,\boldsymbol{\epsilon}_j,\boldsymbol{\epsilon}_2;J_g,J_e)$ are geometric factors and depend solely on the polarization unit vectors of the electric fields $\boldsymbol{\epsilon}_j$ and the total angular momentum quantum numbers J_e and J_g. The dimensionless weighting factors $W_{13}(\omega)$ and $W_{31}(\omega)$ of Eq. (4) are defined as

$$W_{13}(\omega) = \frac{L_{12}^g(\omega) + L_{32}^e(\omega)}{\mathscr{L}(\omega)} \tag{5a}$$

and

$$W_{31}(\omega) = \frac{L_{32}^g(\omega) + L_{12}^e(\omega)}{\mathscr{L}(\omega)}, \tag{5b}$$

and they satisfy the condition

$$W_{13}(\omega) + W_{31}(\omega) = 1. \tag{6}$$

Equation (2) is the key result of this section and expresses the DFWM signal intensity as a product of a concentration part, ΔN^2, a one-photon molecular part, B_{ge}^4, a line shape part, $|\mathscr{L}(\omega)|^2$, and a laboratory-frame geometric part, $|G_F^T|^2$. These quantities relate to different aspects of the experiment, and the DFWM signal intensity is directly proportional to them.

The Einstein absorption coefficients describe the strength of the interaction of the molecule with the excitation fields in the molecular frame. These coefficients can be related to other molecular parameters such as the absorption cross section, the oscillator strength, the line strength, the spontaneous emission lifetime, and the transition-dipole moment.[42] The literature provides an extensive theoretical and experimental data base of these parameters. The physical interpretation of the geometric factors $G_F(\boldsymbol{\epsilon}_4,\boldsymbol{\epsilon}_i,\boldsymbol{\epsilon}_j,\boldsymbol{\epsilon}_2;J_g,J_e)$ is given in Sec. III. The crucial point here is that these factors are just real numbers that account for the geometry of the interaction of the molecule with the electric fields in the laboratory frame. These terms are given in Table I for the allowed polarization configurations of circularly and linearly polarized light for the phase matching geometries of Fig. 1. The angle θ in Fig. 1 is small, usually less than 2°, so we assume that all of the electric fields involved in the DFWM process (excitation and signal) propagate along the space-fixed Z axis. The collinear beam approximation in turn restricts the electric fields to lie in the space-fixed XY plane, and we use the following conventions: R for right circularly polarized, L for left circularly polarized, X for $\phi=0$ linearly polarized, and Y for $\phi=\pi/2$ linearly polarized (Fig. 4). Finally, the line shape functions $L_{j2}^n(\omega)$ are defined as

$$L_{j2}^n(\omega) = \int \frac{f(\mathbf{v})d^3\mathbf{v}}{[(\mathbf{k}_j-\mathbf{k}_2)\cdot\mathbf{v}-i\Gamma_n]} \left\{ \frac{1}{[\omega_0-\omega+\mathbf{k}_j\cdot\mathbf{v}-i\Gamma_{eg}]} - \frac{1}{[\omega_0-\omega+\mathbf{k}_2\cdot\mathbf{v}+i\Gamma_{eg}]} \right\} \frac{1}{[\omega_0-\omega+\mathbf{k}_4\cdot\mathbf{v}-i\Gamma_{eg}]} \tag{7}$$

TABLE I. Geometric factors for circular and linear polarization combinations with the following conventions: R for right circular polarization; L for left circular polarization; X for $\phi=0$ linear polarization; and, Y for $\phi=\pi/2$ linear polarization. Permuting $R\leftrightarrow L$ or $X\leftrightarrow Y$ does not change the values of the geometric factors.

	P Branch		Q Branch		R Branch	
$\epsilon_4\epsilon_i\epsilon_j\epsilon_2$	$G_F(\epsilon_4,\epsilon_i,\epsilon_j,\epsilon_2;J,J-1)$	High-J limit	$G_F(\epsilon_4,\epsilon_i,\epsilon_j,\epsilon_2;J,J)$	High-J limit	$G_F(\epsilon_4,\epsilon_i,\epsilon_j,\epsilon_2;J,J+1)$	High-J limit
$RRRR$	$\frac{1}{15}\frac{(6J^2-1)}{J(2J-1)}$	$\frac{1}{5}$	$\frac{1}{15}\frac{(2J^2+2J+1)}{J(J+1)}$	$\frac{2}{15}$	$\frac{1}{15}\frac{(6J^2+12J+5)}{(2J+3)(J+1)}$	$\frac{1}{5}$
$RLRL$	$\frac{1}{30}\frac{(2J^2-5J+3)}{J(2J-1)}$	$\frac{1}{30}$	$\frac{1}{30}\frac{(4J^2+4J-3)}{J(J+1)}$	$\frac{2}{15}$	$\frac{1}{30}\frac{(2J^2+9J+10)}{(2J+3)(J+1)}$	$\frac{1}{30}$
$RRLL$	$\frac{1}{30}\frac{(2J^2+5J+3)}{J(2J-1)}$	$\frac{1}{30}$	$\frac{1}{30}\frac{(4J^2+4J-3)}{J(J+1)}$	$\frac{2}{15}$	$\frac{1}{30}\frac{(2J^2-J)}{(2J+3)(J+1)}$	$\frac{1}{30}$
$YYYY$	$\frac{1}{15}\frac{(4J^2+1)}{J(2J-1)}$	$\frac{2}{15}$	$\frac{1}{15}\frac{(3J^2+3J-1)}{J(J+1)}$	$\frac{1}{5}$	$\frac{1}{15}\frac{(4J^2+8J+5)}{(2J+3)(J+1)}$	$\frac{2}{15}$
$YXYX$	$\frac{1}{30}\frac{(6J^2-5J-1)}{J(2J-1)}$	$\frac{1}{10}$	$\frac{1}{30}\frac{(2J^2+2J+1)}{J(J+1)}$	$\frac{1}{15}$	$\frac{1}{30}\frac{(6J^2+17J+10)}{(2J+3)(J+1)}$	$\frac{1}{10}$
$YYXX$	$\frac{1}{30}\frac{(6J^2+5J-1)}{J(2J-1)}$	$\frac{1}{10}$	$\frac{1}{30}\frac{(2J^2+2J+1)}{J(J+1)}$	$\frac{1}{15}$	$\frac{1}{30}\frac{(6J^2+7J)}{(2J+3)(J+1)}$	$\frac{1}{10}$
$YXXY$	$-\frac{2}{15}\frac{(J^2-1)}{J(2J-1)}$	$-\frac{1}{15}$	$\frac{1}{15}\frac{(J^2+J-2)}{J(J+1)}$	$\frac{1}{15}$	$-\frac{2}{15}\frac{(J^2+2J)}{(2J+3)(J+1)}$	$-\frac{1}{15}$

where $f(\mathbf{v})$ is the normalized (Maxwell–Boltzmann) velocity-distribution function, $\hbar\omega_0$ is the energy difference between the e and g levels, and $2\Gamma_{eg}$ is the homogeneous full-width (no Doppler broadening) of a dipolar transition between the e and g levels. The sub- and superscripts on L refer to the first terms of Eq. (7). Specifically for the line shape function $L^n_{j2}(\omega)$, n is the quantum-state label of Γ_n where $1/\Gamma_n$ is the total lifetime of the n^{th} level, and j is the field label, either 1 or 3, that corresponds to the $\mathbf{k}$ vector difference $\Delta\mathbf{k}_{j2}=(\mathbf{k}_j-\mathbf{k}_2)$. As written, the specific collisional rates are dependent on temperature but independent of velocity. The velocity integration of Eq. (7) has been performed by many authors[10,29–31,40,43] and is not discussed here.

Effects resulting from finite laser bandwidths and velocity changing collisions are not included in Eq. (7), and to our knowledge, have not been treated. Furthermore, only collisional relaxation is considered (no spontaneous emission), and we assume that the collisional relaxation of the population, the orientation, and the alignment can be represented by a single rate Γ_n. This "single relaxation" assumption is often valid; however, in experiments where efficient energy transfer collision partners such as water are absent, levels characterized by low values of $\mathbf{J}$ may relax with multiple rates and Eq. (2) no longer applies. This topic is discussed in Sec. III C.

In Eq. (4), the geometric factors are weighted by the line shape functions defined in Eq. (7). Therefore, the total DFWM polarization dependence for a given experiment is sensitive to more than the polarizations of the excitation fields; it is also sensitive to the phase matching geometry, the velocity distribution of the absorbing molecules, and the collisional dynamics caused by the environment. This interdependence is an important aspect of DFWM.

For many cases the two geometric factors of Eq. (4) are equal or equally weighted. In these situations the total geometric factor becomes

$$G_F^T(\epsilon_4,\epsilon_1,\epsilon_3,\epsilon_2;J_g,J_e;\omega)=G_F^T(\epsilon_4,\epsilon_1,\epsilon_3,\epsilon_2;J_g,J_e)$$
$$=\tfrac{1}{2}\left[G_F(\epsilon_4,\epsilon_1,\epsilon_3,\epsilon_2;J_g,J_e)+G_F(\epsilon_4,\epsilon_3,\epsilon_1,\epsilon_2;J_g,J_e)\right] \quad (8)$$

and is independent of the velocity distribution of the absorbing molecules and the collisional dynamics caused by the environment. All of this information is then contained exclusively in the total line shape function $\mathscr{S}(\omega)$! This is a powerful result because the DFWM polarization dependence has been disentangled from the collisional dynamics of the experimental environment and depends only on the polarization states of the incident fields and the total angular momentum of the levels involved. Equation (8) has been evaluated for

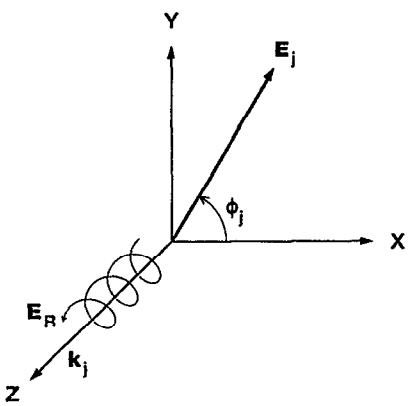

FIG. 4. Electric field vectors $\mathbf{E}_j$ and $\mathbf{E}_R$ in the laboratory frame for linear and right circular polarized light waves, respectively. The propagation direction is the Z axis.

TABLE II. Total geometric factors for FB-DFWM and for BB-, PC-DFWM when Eq. (8) is valid. The conventions are the same as Table I, and permuting $R \leftrightarrow L$ or $X \leftrightarrow Y$ does not change the values of the total geometric factors.

	P Branch		Q Branch		R Branch	
$\epsilon_4\epsilon_i\epsilon_j\epsilon_2$	$G_F^T(\epsilon_4,\epsilon_1,\epsilon_3,\epsilon_2;J,J-1)$	High-J limit	$G_F^T(\epsilon_4,\epsilon_1,\epsilon_3,\epsilon_2;J,J)$	High-J limit	$G_F^T(\epsilon_4,\epsilon_1,\epsilon_3,\epsilon_2;J,J+1)$	High-J limit
$RRRR$	$\frac{1}{15}\frac{(6J^2-1)}{J(2J-1)}$	$\frac{1}{5}$	$\frac{1}{15}\frac{(2J^2+2J+1)}{J(J+1)}$	$\frac{2}{15}$	$\frac{1}{15}\frac{(6J^2+12J+5)}{(2J+3)(J+1)}$	$\frac{1}{5}$
$RLRL$	$\frac{1}{30}\frac{(2J^2+3)}{J(2J-1)}$	$\frac{1}{30}$	$\frac{1}{30}\frac{(4J^2+4J-3)}{J(J+1)}$	$\frac{2}{15}$	$\frac{1}{30}\frac{(2J^2+4J+5)}{(2J+3)(J+1)}$	$\frac{1}{30}$
$RRLL$	$\frac{1}{30}\frac{(2J^2+3)}{J(2J-1)}$	$\frac{1}{30}$	$\frac{1}{30}\frac{(4J^2+4J-3)}{J(J+1)}$	$\frac{2}{15}$	$\frac{1}{30}\frac{(2J^2+4J+5)}{(2J+3)(J+1)}$	$\frac{1}{30}$
$YYYY$	$\frac{1}{15}\frac{(4J^2+1)}{J(2J-1)}$	$\frac{2}{15}$	$\frac{1}{15}\frac{(3J^2+3J-1)}{J(J+1)}$	$\frac{1}{5}$	$\frac{1}{15}\frac{(4J^2+8J+5)}{(2J+3)(J+1)}$	$\frac{2}{15}$
$YXYX$	$\frac{1}{30}\frac{(6J^2-1)}{J(2J-1)}$	$\frac{1}{10}$	$\frac{1}{30}\frac{(2J^2+2J+1)}{J(J+1)}$	$\frac{1}{15}$	$\frac{1}{30}\frac{(6J^2+12J+5)}{(2J+3)(J+1)}$	$\frac{1}{10}$
$YYXX$	$\frac{1}{30}\frac{(6J^2-1)}{J(2J-1)}$	$\frac{1}{10}$	$\frac{1}{30}\frac{(2J^2+2J+1)}{J(J+1)}$	$\frac{1}{15}$	$\frac{1}{30}\frac{(6J^2+12J+5)}{(2J+3)(J+1)}$	$\frac{1}{10}$
$YXXY$	$-\frac{2}{15}\frac{(J^2-1)}{J(2J-1)}$	$-\frac{1}{15}$	$\frac{1}{15}\frac{(J^2+J-2)}{J(J+1)}$	$\frac{1}{15}$	$-\frac{2}{15}\frac{(J^2+2J)}{(2J+3)(J+1)}$	$-\frac{1}{15}$

all allowed polarization configurations for circularly and linearly polarized light, and the results are given in Table II as a function of transition type using the same conventions as in Table I.

The total geometric factors of Table II can be related to what is more commonly referred to as four-wave mixing line strength factors $S_{\mathrm{FWM}}(\epsilon_4,\epsilon_1,\epsilon_3,\epsilon_2;J_g,J_e)$[33,36,37] by

$$S_{\mathrm{FWM}}(\epsilon_4,\epsilon_1,\epsilon_3,\epsilon_2;J_g,J_e) = (S^R_{J_gJ_e})^2 G_F^T(\epsilon_4,\epsilon_1,\epsilon_3,\epsilon_2;J_g,J_e)/(2J_g+1), \tag{9}$$

where $S^R_{J_gJ_e}$ is the molecular rotational line strength (Hönl–London factor) for a one-photon transition[3] and $G_F^T(\epsilon_4,\epsilon_1,\epsilon_3,\epsilon_2;J_g,J_e)$ is defined in Eq. (8). In the general case, population distributions cannot be extracted using the line strength factors of Eq. (9), because the total geometric factor depends on the line shape functions, i.e., the overall DFWM polarization response depends on more than the polarization of the excitation fields.

In our discussion of polarization effects, it is useful to derive expressions that relate how observed DFWM signals vary for a given transition as the polarization of the excitation fields is varied. This variation in DFWM signals is best expressed in terms of a polarization ratio defined as

$$P\left(\frac{\epsilon_4',\epsilon_1',\epsilon_3',\epsilon_2'}{\epsilon_4,\epsilon_1,\epsilon_3,\epsilon_2}\right) = \frac{I'_{\mathrm{DFWM}}}{I_{\mathrm{DFWM}}} \tag{10}$$

which is merely the ratio of the DFWM signal intensities for two different polarization configurations in which all other aspects of the experiment are the same. The three fundamental polarization ratios for circularly and linearly polarized light derived using the values of Table II in Eq. (10) are given in Table III. Note that more ratios can be formed by permuting $R \leftrightarrow L$ and $X \leftrightarrow Y$, but they are identical to those given in Table III. The polarization ratios rapidly approach a high-J limit, and therefore, these values generally describe

TABLE III. Polarization ratios[a] calculated using the values of Table II with $J=J_g$.

	P Branch	High-J limit	Q Branch	High-J limit	R Branch	High-J limit
$P(\mathrm{I})$	$\frac{1}{4}\left[\frac{(J^2-1)}{(J^2+1/4)}\right]^2$	$\frac{1}{4}$	$\frac{1}{9}\left[\frac{(J^2+J-2)}{(J^2+J-1/3)}\right]^2$	$\frac{1}{9}$	$\frac{1}{4}\left[\frac{(J^2+2J)}{(J^2+2J+5/4)}\right]^2$	$\frac{1}{4}$
$P(\mathrm{II})$	$\frac{9}{16}\left[\frac{(J^2-1/6)}{(J^2+1/4)}\right]^2$	$\frac{9}{16}$	$\frac{1}{9}\left[\frac{(J^2+J+1/2)}{(J^2+J-1/3)}\right]^2$	$\frac{1}{9}$	$\frac{9}{16}\left[\frac{(J^2+2J+5/6)}{(J^2+2J+5/4)}\right]^2$	$\frac{9}{16}$
$P(\mathrm{III})$	$\frac{1}{36}\left[\frac{(J^2+3/2)}{(J^2-1/6)}\right]^2$	$\frac{1}{36}$	$\left[\frac{(J^2+J-3/4)}{(J^2+J+1/2)}\right]^2$	1	$\frac{1}{36}\left[\frac{(J^2+2J+5/2)}{(J^2+2J+5/6)}\right]^2$	$\frac{1}{36}$

[a] $P(\mathrm{I}) = PP\left(\frac{YXXY}{YYYY}\right), P(\mathrm{II}) = P\left(\frac{YXYX}{YYYY}\right) = P\left(\frac{YYXX}{YYYY}\right) = \frac{1}{4}P\left(\frac{RRRR}{YYYY}\right)$, and $P(\mathrm{III}) = P\left(\frac{RLRL}{RRRR}\right) = \frac{1}{4}P\left(\frac{RLRL}{YXYX}\right) = \frac{1}{4}P\left(\frac{RLRL}{YYXX}\right) = P\left(\frac{RRLL}{RRRR}\right) = \frac{1}{4}P\left(\frac{RRLL}{YXYX}\right) = \frac{1}{4}P\left(\frac{RRLL}{YYXX}\right)$.

the DFWM signal variation, as the polarization configuration is changed for those systems for which Eq. (8) is valid.

We turn to a discussion of specific experimental conditions in which we point out the cases for which Eq. (4) reduces to Eq. (8). Here, we invoke the grating picture of DFWM to gain some insight as to the relative magnitude of the line shape functions $L^n_{j2}(\omega)$. The grating picture of DFWM involves the interference of the excitation fields. When the excitation fields are tuned to a one-photon resonance, the interference between two of the fields, $\mathbf{E}_2$ and $\mathbf{E}_j$ ($j=1$ or 3), leads to a spatial modulation in the (complex) refractive index and hence forms a grating that can scatter the third field into a fourth field (DFWM signal).[10,44] The grating is characterized by the grating k-vector, $\Delta\mathbf{k}_{j2}=(\mathbf{k}_j-\mathbf{k}_2)$, which describes the grating's orientation and spacing in the laboratory frame. The grating spacing D_{j2} is given by

$$D_{j2}=\frac{2\pi}{|\Delta\mathbf{k}_{j2}|}=\frac{\lambda}{2\sin(\theta/2)} \tag{11}$$

where $|\Delta\mathbf{k}_{j2}|$ is the magnitude of the grating k vector and θ is the angle between the two propagation vectors, $\mathbf{k}_j$ and $\mathbf{k}_2$, of the fields forming the grating ($0\leqslant\theta\leqslant\pi$). When θ is small the grating spacing is large, and when θ is large the grating spacing is small. If the absorbers involved in forming the grating are moving, such as in a gas, the grating with the smallest spacing is "washed out" to a higher degree when Doppler broadening is significant.[45] This argument is useful in predicting the general DFWM polarization dependence and is substantiated by evaluating the integrals of Eq. (7).[43]

B. Phase matching geometry 1: Forward box DFWM (FB-DFWM)

We are prepared to consider the polarization effects for specific phase matching geometries and the relative sensitivity of these effects to the collisional environment. For the FB-DFWM geometry of Fig. 1, all fields are nearly copropagating, $\theta\cong 0$, and $|\Delta\mathbf{k}_{12}|=|\Delta\mathbf{k}_{32}|\cong 0$. Therefore, all the gratings formed in the FB-DFWM phase matching geometry have large grating spacings, $D_{12}=D_{32}\rightarrow\infty$, and

$$L^g_{12}(\omega)=L^g_{32}(\omega);\quad L^e_{12}(\omega)=L^e_{32}(\omega). \tag{12}$$

Substituting Eq. (12) into Eqs. (5a) and (5b) shows that geometric factors that correspond to the interchange of the two pump fields (1 and 3) are equally weighted. The total geometric factor has the simple form of Eq. (8) for all transition types and polarization configurations. Therefore, Tables II and III contain all of the relevant polarization information for FB-DFWM. As shown in Table III, the polarization ratios are equal for any entry with orthogonally polarized pump fields ($\boldsymbol{\epsilon}_1\cdot\boldsymbol{\epsilon}_3^*=0$). This result distinguishes the FB-DFWM configuration from the other configurations as we shall see below. This distinction is in addition to the fact that FB-DFWM is not a sub-Doppler spectroscopic technique.

C. Phase matching geometries 2 and 3: Backward box and phase conjugate DFWM (BB- and PC-DFWM)

For the BB-DFWM and PC-DFWM geometries of Fig. 1, fields 1 and 2 are nearly copropagating, $|\Delta\mathbf{k}_{12}|\cong 0$, and fields 3 and 2 are nearly counterpropagating, $|\Delta\mathbf{k}_{32}|\cong 2k=4\pi/\lambda$. Therefore, two types of gratings are formed in these phase matching geometries: one has a large grating spacing, $D_{12}\rightarrow\infty$; and the other has a small spacing, $D_{32}\rightarrow\lambda/2$. Allowing for more wash out of the small-spaced grating compared to the large-spaced grating when the molecules are moving, we may write the following inequalities:

$$L^g_{12}(\omega)\geqslant L^g_{32}(\omega);\quad L^e_{12}(\omega)\geqslant L^e_{32}(\omega). \tag{13}$$

Unlike for FB-DFWM, the total geometric factors for BB- and PC-DFWM that correspond to the interchange of the two pump fields (1 and 3) are generally not weighted equally. Hence the overall DFWM polarization response, i.e., the total geometric factor $G^T_F(\boldsymbol{\epsilon}_4,\boldsymbol{\epsilon}_1,\boldsymbol{\epsilon}_3,\boldsymbol{\epsilon}_2;J_g,J_e;\omega)$ of Eq. (4), will be sensitive to the collisional environment because the weighting factors $W_{13}(\omega)$ and $W_{31}(\omega)$ are dependent on the relative relaxation rates of the g and e levels. This dependence complicates the interpretation of DFWM spectra for these phase matching geometries, and the weighted average expressed in Eq. (4) generally must be performed.

In some cases, however, the polarization dependence for BB- and PC-DFWM can be disentangled from collisional effects. These cases arise when

$$G_F(\boldsymbol{\epsilon}_4,\boldsymbol{\epsilon}_1,\boldsymbol{\epsilon}_3,\boldsymbol{\epsilon}_2;J_g,J_e)=G_F(\boldsymbol{\epsilon}_4,\boldsymbol{\epsilon}_3,\boldsymbol{\epsilon}_1,\boldsymbol{\epsilon}_2;J_g,J_e) \tag{14a}$$

or when

$$\Gamma_g=\Gamma_e\Rightarrow L^g_{12}(\omega)=L^e_{12}(\omega);\quad L^g_{32}(\omega)=L^e_{32}(\omega). \tag{14b}$$

For these cases Eq. (4) reduces to Eq. (8), and again, the DFWM polarization response only depends on the polarization states of the incident fields and the total angular momentum of the levels involved. Equation (14a) is satisfied for all Q branch ($\Delta J=0$) transitions and for P branch ($\Delta J=-1$) and R branch ($\Delta J=+1$) transitions when the two pump fields are of the same polarization ($\boldsymbol{\epsilon}_1\cdot\boldsymbol{\epsilon}_3^*=1$). Therefore, the simple results of Tables II and III can be used to evaluate BB- and PC-DFWM signal intensities for Q-branch transitions and for P- and R-branch transitions when $\boldsymbol{\epsilon}_1\cdot\boldsymbol{\epsilon}_3^*=1$ in addition to FB-DFWM signal intensities. For P- and R-branch transitions with orthogonally polarized pump fields ($\boldsymbol{\epsilon}_1\cdot\boldsymbol{\epsilon}_3^*=0$), however, Eq. (14b) must be satisfied for the results of Tables II and III to apply, i.e., the upper and lower levels must relax at the same rate. If neither Eq. (14a) nor Eq. (14b) is satisfied, the DFWM polarization response depends on the dynamics of the collisional environment under study. This drawback is offset because collisional relaxation information can be obtained from polarization-ratio measurements without having to resolve spectral line shapes.[17,46]

Grating wash out leading to the inequality in Eq. (13) often occurs for Doppler-broadened systems in which the homogeneous full-width $2\Gamma_{eg}$ of the spectroscopic transition between levels e and g is smaller than the Doppler width $\Delta\omega_D$. Experiments conducted under low-pressure, high-

temperature conditions, such as atmospheric-pressure (and lower) flames and plasmas, are examples of Doppler-broadened systems. Again invoking the grating picture of DFWM for this case yields $L^g_{12} > L^g_{32}$ and $L^e_{12} > L^e_{32}$; in other words, the small-spaced grating is washed out more than the large-spaced grating. Substituting these inequalities into Eq. (4) shows that P- and R-branch transitions with orthogonally polarized pump fields are sensitive to differences in the relaxation rates of the g and e levels. To emphasize this point consider the case when $\Gamma_g < \Gamma_e$. Given two orthogonal polarization states ϵ' and ϵ'', we have

$$G_F^T(\epsilon', \epsilon', \epsilon'', \epsilon''; J_g, J_e; \omega) > G_F^T(\epsilon', \epsilon'', \epsilon', \epsilon''; J_g, J_e; \omega) \tag{15a}$$

for P-branch ($\Delta J = -1$) transitions, and

$$G_F^T(\epsilon', \epsilon', \epsilon'', \epsilon''; J_g, J_e; \omega) < G_F^T(\epsilon', \epsilon'', \epsilon', \epsilon''; J_g, J_e; \omega) \tag{15b}$$

for R-branch ($\Delta J = +1$) transitions. If $\Gamma_g > \Gamma_e$, the inequalities of Eqs. (15a) and (15b) are reversed. These inequalities hold for frequency-integrated DFWM signal intensities as well. Analytic expressions for the line shape functions in the Doppler-broadened limit are found in Refs. 10, 30, and 43 and can be used to quantify the inequalities of Eqs. (15a) and (15b).

Recall that for P- and R-branch transitions with $\Gamma_g = \Gamma_e$, the total geometric factor is invariant to the exchange of the polarizations of the pump fields. This result is important because even though most flame and plasma experiments are Doppler-broadened, diagnostic applications typically involve the investigation of molecular species in which rotational energy transfer collisions are the dominant type of collision. Furthermore, the energy-level spacings of the g and e levels of these species are usually similar, and as a result, they have similar rotational energy transfer rates. For these experiments, $\Gamma_g \cong \Gamma_e$, and to a first approximation, the simple results of Tables II and III describe the DFWM polarization response. This response is discussed in detail in WZR2 for the case of the CH radical in an atmospheric-pressure flame.

We conclude this discussion by considering systems in the homogeneously broadened limit, i.e., $2\Gamma_{eg} \gg \Delta\omega_D$. Experiments performed in supercritical water[47] that are characterized by high pressure (~218 atm) and relatively low temperature (~647 K) closely approximate this limit. In this limit $L^g_{12}(\omega) \cong L^g_{32}(\omega)$ and $L^e_{12}(\omega) \cong L^e_{32}(\omega)$ because the absorbers are effectively relaxed before they have a chance to move, and thus neither the large- nor small-spaced gratings are washed out. Therefore, for homogeneously broadened systems Eq. (4) reduces to Eq. (8), and the results presented in Tables II and III apply. For a more precise evaluation of Eq. (4), Wandzura[48] obtained analytic expressions for the line shape functions in this limit that can be used to calculate the DFWM polarization dependence.

D. Other signal contributions

The discussion above assumes that no other process contributes to the DFWM signal. For some experimental conditions, however, other types of laser-induced grating phenomena[44] can coherently scatter light along the DFWM signal direction. The most likely candidate is a thermal grating that results from the localized absorption of the laser energy and subsequent heating of the medium. This absorption leads to a spatial-density modulation in gases that can produce signals on the order of or greater than the DFWM response under some conditions.[46,49,50] Another intensity grating effect observed at high laser intensities is an electrostrictive grating[51] that results from an electric-field induced modulation in the gas density. These types of effects, however, can result only from the interference of two fields that have the same polarization (intensity gratings); *fields with orthogonal polarizations do not produce such effects* (polarization gratings) because there is no spatial modulation of the field intensity (only its polarization is spatially modulated).[52,53] If the molecule is optically active (chiral), however, then circular-dichroism induced thermal gratings can be formed with orthogonally polarized fields.[54]

If other types of gratings are present, polarization dependences different from those discussed above are observed. In particular, polarization configurations that involve large-spaced intensity gratings have anomalous signal intensities if additional intensity grating contributions are present. A good way to test for this effect is to measure the polarization ratio of a Q-branch transition with orthogonally polarized pump fields in the BB- or PC-DFWM phase matching geometry. If the polarization ratio is not unity, another process is likely to be contributing.[17] Rahn and Brown[46] used similar polarization techniques to determine that thermal gratings make significant contributions to OH spectra taken in atmospheric-pressure flames. If other gratings are determined to be contributing, the *YXXY* polarization configuration best discriminates against their contribution for all experimental conditions, but the *YYXX* and *RRLL* configurations are also good choices for Doppler-broadened systems with grating wash out because only small-spaced intensity gratings are present.

E. Influence of hyperfine structure

A full treatment considering the influence of hyperfine structure is possible,[31,35] but the additional complexity required to include such effects is not warranted[2,55] for the conditions described in this paper, i.e., the spectroscopy of molecular systems in collisionally dominated environments. This conclusion can be justified by invoking the vector model of angular momenta. In the absence of collisions, the rotational angular momentum **J** couples to the nuclear angular momentum **I** to form the total angular momentum **F** so that the prepared direction of **J** in the laboratory frame is lost to some degree (depolarized). This directional blurring obviously influences the geometric factors related to the distribution of **J** in the laboratory frame. If the magnitude of **J** is substantially larger than the magnitude of **I** (typically **I** takes values up to about 5/2), **J** and **F** will be close to parallel, and the hyperfine depolarization will be small. This condition is usually satisfied for DFWM spectra of molecular species in which the magnitude of **J** for the levels of interest is much larger than the magnitude of **I**. However, for low values of **J** (magnitudes of **J** close to or smaller than those of **I**), the hyperfine depolarization can be significant.

If **J** is effectively decoupled from **I** by collisions, the hyperfine depolarization is small even for low **J** values. We used time-independent diagrammatic perturbation theory to derive the results of this paper, which implies that the results are valid for low-intensity, steady-state conditions in which population transfer is assumed to be small. Inherent in this approximation is the fact that the population relaxation and collisional dephasing times must be much shorter than the temporal duration of the laser pulse. These collisional times are typically much shorter than the precessional period of **J** about **F** (usually tens of nanoseconds or longer), which implies that hyperfine depolarization will not be significant for collisionally dominated systems. A quick experimental check is to determine if the hyperfine structure is spectrally resolved in either the BB- or PC-DFWM (sub-Doppler) phase matching geometries. If it is not resolved, hyperfine interactions will not significantly affect the results presented here. This conclusion follows because unresolved hyperfine structure suggests that the hyperfine splitting is small compared with the collisional broadening of the hyperfine components, which in turn implies that the precessional period of **J** about **F** is slow compared with the time it takes to collisionally decouple **J** from **I**.

III. INTERPRETATION OF THE DFWM SIGNAL INTENSITY IN TERMS OF MULTIPOLE MOMENTS

A. Derivation and general expressions

In DFWM two molecular levels with total angular momentum quantum numbers J_g and J_e, respectively, are coupled by the input fields. Describing the resulting coherence between these levels in terms of the total angular momentum distribution is convenient. The most complete description of the angular momentum distribution is in terms of state multipoles that represent the populations of the levels and the coherences existing between them.[56,57] The state multipoles are spherical tensors of rank K and component $Q(-K \leq Q \leq K)$. The $Q=0$ components describe the projection of **J** onto the space-fixed Z axis, and the $Q \neq 0$ components describe the projection of **J** onto the space-fixed XY plane. Here the monopole term ($K=0$) is proportional to the population. All odd rank multipoles (dipole, octopole, etc.) describe the orientation of the angular momentum, and all even rank multipoles (quadrupole, hexadecapole, etc.) are related to the alignment of the angular momentum. Below we show that the highest allowed value of K for unsaturated DFWM is 2. Therefore, we take the $K=0$, 1, and 2 terms to describe the (scalar) population, (dipolar) orientation, and (quadupolar) alignment, respectively.

We outline a method for calculating the third-order nonlinear polarization for fully resonant DFWM of molecular gases in collisionally dominated environments. The expressions are derived using diagrammatic perturbation theory[40,41,58,59] and are evaluated using a spherical tensor formalism.[3,60,61] The techniques used are standard; consequently, only the key elements of the derivation are presented. In what follows beam propagation effects are ignored because it is assumed that the absorption of the incident beams is negligibly small.

The molecular levels are coupled by three input electric fields. The intensity of each electric field $\mathbf{E}_j(\mathbf{r},t)$ is given by

$$I_j = \epsilon_0 c \langle |\mathbf{E}_j(\mathbf{r},t)|^2 \rangle = \frac{\epsilon_0 c}{2} |\mathscr{E}_j|^2, \tag{16}$$

where the angular brackets denote a cycle average and j is the field label, ϵ_0 is the permittivity of free space, c is the speed of light, and $\mathscr{E}_j$ is the scalar amplitude of the electric field. The result of the interaction of the three electric fields with the molecular sample is the generation of the third-order electric polarization $\mathbf{P}^{(3)}(\mathbf{r},t)$. We note that many conventions are used for expressing $\mathbf{P}^{(3)}(\mathbf{r},t)$. Therefore, for clarity, we follow the convention of Butcher and Cotter[62] throughout and write $\mathbf{P}^{(3)}(\mathbf{r},t)$ in SI units as

$$\begin{aligned} &\mathbf{P}^{(3)}(\mathbf{r},t) = \tfrac{1}{2}\, \mathbf{P}^{(3)}_{\mathrm{DFWM}} e^{-i(\omega_4 t - \mathbf{k}_4 \cdot \mathbf{r})} + \text{c.c.}; \\ &\mathbf{P}^{(3)}_{\mathrm{DFWM}} = \mathscr{P}^{(3)}_{\mathrm{DFWM}} \boldsymbol{\epsilon}_4, \end{aligned} \tag{17}$$

where $\mathbf{P}^{(3)}_{\mathrm{DFWM}}$ is the vector amplitude, and $\mathscr{P}^{(3)}_{\mathrm{DFWM}}$ is the scalar amplitude, and $\boldsymbol{\epsilon}_4$ is the normalized ($\boldsymbol{\epsilon}_4 \cdot \boldsymbol{\epsilon}_4^* = 1$) polarization vector. $\mathbf{P}^{(3)}_{\mathrm{DFWM}}$ is defined in terms of the DFWM third-order nonlinear susceptibility $\boldsymbol{\chi}^{(3)}_{\mathrm{DFWM}}(-\omega_4,\omega_1,\omega_3,-\omega_2)$ as

$$\mathbf{P}^{(3)}_{\mathrm{DFWM}} = \epsilon_0\, \tfrac{3}{4}\, \boldsymbol{\chi}^{(3)}_{\mathrm{DFWM}}(-\omega_4,\omega_1,\omega_3,-\omega_2) \vdots \mathbf{E}_1 \mathbf{E}_2^* \mathbf{E}_3. \tag{18}$$

where the symbol $\vdots$ refers to tensor contraction. The DFWM signal intensity is proportional to the cycle average of the absolute square of the third-order nonlinear polarization. In analogy with Eq. (16), the DFWM signal intensity is proportional to the absolute value squared of the scalar amplitude $\mathscr{P}^{(3)}_{\mathrm{DFWM}}$, i.e.,

$$I_{\mathrm{DFWM}} = I_4 \propto \langle |\mathbf{P}^{(3)}(\mathbf{r},t)|^2 \rangle = \tfrac{1}{2} |\mathscr{P}^{(3)}_{\mathrm{DFWM}}|^2. \tag{19}$$

Therefore our concern is to calculate $\mathscr{P}^{(3)}_{\mathrm{DFWM}}$ where

$$\begin{aligned} \mathscr{P}^{(3)}_{\mathrm{DFWM}} = \mathbf{P}^{(3)}_{\mathrm{DFWM}} \cdot \boldsymbol{\epsilon}_4^* = \epsilon_0\, \tfrac{3}{4} \\ \times \chi^{(3)}_{\mathrm{DFWM}}(-\omega_4,\omega_1,\omega_3,-\omega_2) \mathscr{E}_1 \mathscr{E}_2^* \mathscr{E}_3 \end{aligned} \tag{20}$$

and $\chi^{(3)}_{\mathrm{DFWM}}(-\omega_4,\omega_1,\omega_3,-\omega_2)$ is the scalar form of the third-order susceptibility. (See Ref. 62, p. 27.)

The significant contributions to the DFWM third-order nonlinear susceptibility are represented using double-sided Feynman diagrams in Fig. 3. Note that 16 diagrams are necessary to account for all of the time orderings that correspond to the energy-level diagram of Fig. 2. These diagrams represent the following expression[33] for $\chi^{(3)}_{\mathrm{DFWM}}(-\omega_4,\omega_1,\omega_3,-\omega_2)$ in the perturbative (weak-field) limit

$$\begin{aligned} &\chi^{(3)}_{\mathrm{DFWM}}(-\omega_4,\omega_1,\omega_3,-\omega_2) \\ &= \frac{1}{6\epsilon_0 \hbar^3} [C(-\omega_4,\omega_1,\omega_3,-\omega_2) \\ &\quad + C(-\omega_4,\omega_3,\omega_1,-\omega_2)], \end{aligned} \tag{21}$$

where

$$C(-\omega_4,\omega_i,\omega_j,-\omega_2)$$

$$=N\Bigg\{\sum_{\text{all } M}\langle g|\boldsymbol{\epsilon}_4^*\cdot\boldsymbol{\mu}|e'\rangle\langle e'|\boldsymbol{\epsilon}_j\cdot\boldsymbol{\mu}|g'\rangle\langle g'|\boldsymbol{\epsilon}_2^*\cdot\boldsymbol{\mu}|e\rangle$$

$$\times\langle e|\boldsymbol{\epsilon}_i\cdot\boldsymbol{\mu}|g\rangle(A-B_1)+\sum_{\text{all } M}\langle e'|\boldsymbol{\epsilon}_j\cdot\boldsymbol{\mu}|g'\rangle$$

$$\times\langle g'|\boldsymbol{\epsilon}_2^*\cdot\boldsymbol{\mu}|e\rangle\langle e|\boldsymbol{\epsilon}_i\cdot\boldsymbol{\mu}|g\rangle\langle g|\boldsymbol{\epsilon}_4^*\cdot\boldsymbol{\mu}|e'\rangle(B_2-B_3)\Bigg\}, \tag{22}$$

and

$$A=(\rho_{gg}^{(0)}-\rho_{ee}^{(0)})\{[\omega_0-\omega+\mathbf{k}_i\cdot\mathbf{v}-i\Gamma_{eg}]$$
$$\times[(\mathbf{k}_i-\mathbf{k}_2)\cdot\mathbf{v}-i\Gamma_{g'g}][\omega_0-\omega+\mathbf{k}_4\cdot\mathbf{v}-i\Gamma_{e'g}]\}^{-1}, \tag{23a}$$

$$B_1=(\rho_{g'g'}^{(0)}-\rho_{ee}^{(0)})\{[\omega_0-\omega+\mathbf{k}_2\cdot\mathbf{v}+i\Gamma_{eg'}]$$
$$\times[(\mathbf{k}_i-\mathbf{k}_2)\cdot\mathbf{v}-i\Gamma_{g'g}][\omega_0-\omega+\mathbf{k}_4\cdot\mathbf{v}-i\Gamma_{e'g}]\}^{-1}, \tag{23b}$$

$$B_2=(\rho_{g'g'}^{(0)}-\rho_{e'e'}^{(0)})\{[\omega_0-\omega+\mathbf{k}_j\cdot\mathbf{v}-i\Gamma_{e'g'}]$$
$$\times[(\mathbf{k}_j-\mathbf{k}_2)\cdot\mathbf{v}-i\Gamma_{e'e}][\omega_0-\omega+\mathbf{k}_4\cdot\mathbf{v}-i\Gamma_{e'g}]\}^{-1}, \tag{23c}$$

and

$$B_3=(\rho_{g'g'}^{(0)}-\rho_{ee}^{(0)})\{[\omega_0-\omega+\mathbf{k}_2\cdot\mathbf{v}+i\Gamma_{eg'}]$$
$$\times[(\mathbf{k}_j-\mathbf{k}_2)\cdot\mathbf{v}-i\Gamma_{e'e}][\omega_0-\omega+\mathbf{k}_4\cdot\mathbf{v}-i\Gamma_{e'g}]\}^{-1}. \tag{23d}$$

In Eq. (22), N is the total number of absorbers, the ket $|n\rangle$ represents the total molecular wave function for the quantum level characterized by total angular momentum $\mathbf{J_n}$, $\boldsymbol{\mu}$ is the electric dipole moment operator, and A, B_1, B_2, and B_3 represent energy-resonant denominators. In Eqs. (23a)–(23d), $\rho_{nn}^{(0)}$ is the initial density matrix element for the magnetic sublevel M_n of the level n and refers to the initial probability of the system being in that sublevel, $\hbar\omega_0$ is the energy difference between the levels e and g, $\mathbf{k}_j$ is the propagation vector of the field label j, $\mathbf{v}$ is the velocity vector of the absorbing molecule, and Γ_{nm} represents the total dephasing rate of the coherence between the magnetic sublevels M_n and M_m.

We seek to evaluate Eqs. (21)–(23) using a spherical tensor formalism and to express the DFWM third-order nonlinear polarization in terms of its multipole components. This method provides a well developed and efficient way of using the inherent symmetry of the system and enables dynamic and geometric factors to be separated from each other. The evaluation is similar to that of coherent LIF by Greene and Zare (GZ)[2] with the exception that four photons are involved. This greater complexity, however, does not significantly increase the difficulty of solving the problem, which illustrates the power of the spherical tensor method.

The first step in the evaluation is to recognize that the summation over projections onto the several degenerate sublevels of the level n constitutes a single projection operator indicated by

$$P=\sum_{M_n}|n\rangle\langle n|=1, \tag{24}$$

which is scalar (tensor of rank 0). Substituting Eq. (24) into the first term of Eq. (22) gives

$$\sum_{M_g}\langle g|\hat{O}|g\rangle, \tag{25}$$

where

$$\hat{O}=(\boldsymbol{\epsilon}_4^*\cdot\boldsymbol{\mu}_4)(\boldsymbol{\epsilon}_j\cdot\boldsymbol{\mu}_j)(\boldsymbol{\epsilon}_2^*\cdot\boldsymbol{\mu}_2)(\boldsymbol{\epsilon}_i\cdot\boldsymbol{\mu}_i), \tag{26}$$

and the energy-resonant denominators have been omitted for simplicity. The transition dipole moment operators $\boldsymbol{\mu}$ have been subscripted for bookkeeping. The tensor product in Eq. (26) has four dipole (rank 1) terms that can be organized in various ways to produce a tensor of rank 4. In DFWM, however, the process initiates and terminates in the same level, denoted here as $|\alpha_n J_n M_n\rangle$, where M_n is the projection of the total angular momentum $\mathbf{J_n}$ (quantum number J_n) on the space-fixed Z axis, and α_n represents all other quantum numbers, i.e., electronic and vibrational. The only operator $\hat{O}$ that can connect the ket $|\alpha_n J_n M_n\rangle$ to the bra $\langle\alpha_n J_n M_n|$ is a scalar, c, i.e.,

$$\langle\alpha_n J_n M_n|\hat{O}|\alpha_n J_n M_n\rangle=\langle\alpha_n J_n M_n|c|\alpha_n J_n M_n\rangle=c \tag{27}$$

because any higher rank tensor will cause the matrix element to vanish. A tensor of rank zero can be formed by contracting tensors of higher and equal rank. For example two tensors of rank 1 (vectors) make a tensor of rank 0 by the vector dot product. Similarly, two vectors of rank two (quadrupoles) can also be contracted. Recall that Eq. (26) has four dipole (rank 1) terms that can be organized in various ways, for instance as a tensor product of three dipoles to form tensors up to rank 3 and a single dipole of rank 1. However, this tensor product cannot be contracted to form a scalar. Therefore, we organize Eq. (26) in terms of tensor products of two dipoles to form tensors up to rank 2 which can be contracted to give a scalar. The resulting expressions are readily interpreted using the grating picture of DFWM. We note here, however, that higher-order tensors will contribute to the DFWM signal as the laser intensity approaches saturation. In a perturbative treatment, an increase in the laser intensity is accounted for by including higher order terms in the perturbative expansion, i.e., χ^5, χ^7, χ^9, $\cdots$ χ^n. These additional terms contain matrix element products with 6, 8, 10, $\cdots$ $n+1$ factors and can form tensors up to rank $(n+1)/2$.

The spherical tensor convention adopted here is that of Zare.[3] Below $\otimes$ refers to the tensor product and $\times$ refers to scalar multiplication. We begin by expressing the vector dot product involved in the electric dipole interaction in spherical tensor notation:

$$(\boldsymbol{\epsilon}\cdot\boldsymbol{\mu})=-\sqrt{3}[\epsilon^{(1)}\otimes\mu^{(1)}]_0^{(0)}=\sum_Q(-1)^Q\epsilon_Q^{(1)}\mu_{-Q}^{(1)}, \tag{28}$$

where the general expression for the scalar product is

$$[T^{(K)}\otimes V^{(K)}]_0^{(0)}=\sum_Q (-1)^{K-Q}(2K+1)^{-1/2}T_Q^{(K)}V_{-Q}^{(K)}. \tag{29}$$

In Eqs. (28) and (29) each vector is written in terms of its spherical tensor components. See the Appendix. The product of two dipole terms is

$$\begin{aligned}(\boldsymbol{\epsilon}_i^*\cdot\boldsymbol{\mu}_i)(\boldsymbol{\epsilon}_j\cdot\boldsymbol{\mu}_j)&=3[[\epsilon_i^{*(1)}\otimes\mu_i^{(1)}]^{(0)}\otimes[\epsilon_j^{(1)}\otimes\mu_j^{(1)}]^{(0)}]_0^{(0)}\\&=3\sum_K\langle(11)K(11)K0|(11)0(11)00\rangle\\&\quad\times\{[\epsilon_i^{*(1)}\otimes\epsilon_j^{(1)}]^{(K)}\otimes[\mu_i^{(1)}\otimes\mu_j^{(1)}]^{(K)}\}_0^{(0)},\end{aligned} \tag{30}$$

where the operators have been regrouped using the recoupling transformation of four angular momenta. The summation over K in Eq. (30) is from $K=0$ to $K=2$ because the tensor product of two dipoles can form a scalar (the dot product), a vector (the cross product), or a tensor of rank 2. The factor in angular brackets is a recoupling coefficient and involves a 9-j symbol, three of whose arguments are zero. This coefficient has been evaluated [GZ Eq. (37)] and has the general form

$$\begin{aligned}&\langle(KK')K''(KK')K''0|(KK)0(K'K')00\rangle\\&\quad=(2K+1)^{-1/2}(2K'+1)^{-1/2}(2K''+1)^{1/2}.\end{aligned} \tag{31}$$

The operator $\hat{O}$ defined in Eq. (26) can be represented using Eqs. (29)–(31) as

$$\begin{aligned}\hat{O}=\sum_{K,K'}&(2K+1)^{1/2}(2K'+1)^{1/2}[[[\epsilon_4^{*(1)}\otimes\epsilon_j^{(1)}]^{(K)}\\&\otimes[\mu_4^{(1)}\otimes\mu_j^{(1)}]^{(K)}]^{(0)}\otimes[[\epsilon_2^{*(1)}\otimes\epsilon_i^{(1)}]^{(K')}\\&\otimes[\mu_2^{(1)}\otimes\mu_i^{(1)}]^{(K')}]^{(0)}]_0^{(0)},\end{aligned} \tag{32}$$

and with one more recoupling transformation all of the polarization factors can be grouped together. Performing this transformation gives

$$\begin{aligned}\hat{O}=\sum_{K,K',K''}&(2K+1)^{1/2}(2K'+1)^{1/2}\\&\times\langle(KK')K''(KK')K''0|(KK)0(K'K')00\rangle\\&\times[[[\epsilon_4^{*(1)}\otimes\epsilon_j^{(1)}]^{(K)}\otimes[\epsilon_2^{*(1)}\otimes\epsilon_i^{(1)}]^{(K')}]^{(K'')}\\&\otimes[[\mu_4^{(1)}\otimes\mu_j^{(1)}]^{(K)}\otimes[\mu_2^{(1)}\otimes\mu_i^{(1)}]^{(K')}]^{(K'')}]_0^{(0)}\end{aligned} \tag{33}$$

which can be simplified using Eq. (31) and expanded in terms of its tensor components by Eq. (29) to yield

$$\begin{aligned}\hat{O}=\sum_{K,K',K'',Q''}&(-1)^{K''-Q''}[[\epsilon_4^{*(1)}\otimes\epsilon_j^{(1)}]^{(K)}\otimes[\epsilon_2^{*(1)}\\&\otimes\epsilon_i^{(1)}]^{(K')}]_{Q'}^{(K'')}[[\mu_4^{(1)}\otimes\mu_j^{(1)}]^{(K)}\otimes[\mu_2^{(1)}\otimes\mu_i^{(1)}]^{(K')}]_{-Q''}^{(K'')}.\end{aligned} \tag{34}$$

Equation (34) is the same as Eq. (39) of GZ for LIF with the important distinction that four different electric fields are involved. Recalling that only a scalar operator, i.e., a tensor of rank $K''=0$, can connect the ket $|\alpha_nJ_nM_n\rangle$ to the bra $\langle\alpha_nJ_nM_n|$, we have $K=K'$ because only two tensors of equal rank can be contracted to form a scalar. Therefore, the summation over K, K', and K'' of Eq. (34) is replaced with a single summation over K. Substituting into Eq. (25) gives a key result, namely,

$$\begin{aligned}&\sum_{M_g}\langle\alpha_gJ_gM_g|\hat{O}|\alpha_gJ_gM_g\rangle\\&\quad=\sum_K\Bigg\{[[\epsilon_4^{*(1)}\otimes\epsilon_j^{(1)}]^{(K)}\otimes[\epsilon_2^{*(1)}\otimes\epsilon_i^{(1)}]^{(K)}]_0^{(0)}\\&\qquad\times\sum_{M_g}\langle\alpha_gJ_gM_g|[[\mu_4^{(1)}\otimes\mu_j^{(1)}]^{(K)}\\&\qquad\otimes[\mu_2^{(1)}\otimes\mu_i^{(1)}]^{(K)}]_0^{(0)}|\alpha_gJ_gM_g\rangle\Bigg\},\end{aligned} \tag{35}$$

where K can have values of 0, 1, and 2 (the range of K and K'), and the shorthand notation for the molecular wave functions $|n\rangle$ has been replaced with $|\alpha_nJ_nM_n\rangle$. Equation (35) displays the disentanglement of the geometric aspects (polarization tensors) of the problem from the dynamics (transition moment tensors) of the electric dipole interaction.

The first factor of Eq. (35) represents the scalar contraction of two polarization tensors to form a scalar and is essentially in its most fundamental form. The explicit evaluation of this factor is straightforward and is shown in the Appendix. The second factor of Eq. (35), on the other hand, can be reduced to a more fundamental form. Applying the Wigner–Eckart theorem [Ref. 3, Eq. (5.14)] yields after some simplification

$$\begin{aligned}&\sum_{M_g}\langle\alpha_gJ_gM_g|[[\mu_4^{(1)}\otimes\mu_j^{(1)}]^{(K)}\\&\quad\otimes[\mu_2^{(1)}\otimes\mu_i^{(1)}]^{(K)}]_0^{(0)}|\alpha_gJ_gM_g\rangle\\&\quad=(2J_g+1)^{1/2}\langle\alpha_gJ_g\|[[\mu_4^{(1)}\otimes\mu_j^{(1)}]^{(K)}\\&\qquad\otimes[\mu_2^{(1)}\otimes\mu_i^{(1)}]^{(K)}]^{(0)}\|\alpha_gJ_g\rangle.\end{aligned} \tag{36}$$

The last factor of Eq. (36) is the reduced matrix element of a

compound tensor operator and can be evaluated using the following relation [Ref. 3, Eq. (5.74)]:

$$\begin{aligned}&\langle \alpha J\|X^{(K)}\|\alpha' J'\rangle \\ &=\langle \alpha J\|[T^{(K_1)}\otimes T^{(K_2)}]^{(K)}\|\alpha' J'\rangle \\ &=(-1)^{K+J+J'}(2K+1)^{1/2}\sum_{\alpha'' J''}\begin{Bmatrix} J' & J' & K \\ K_1 & K_2 & J''\end{Bmatrix} \\ &\quad\times\langle \alpha J\|T^{(K_1)}\|\alpha'' J''\rangle\langle \alpha'' J''\|T^{(K_2)}\|\alpha' J'\rangle, \end{aligned}\tag{37}$$

where the term in curly brackets is a 6-j symbol. Applying Eq. (37) to (36) gives the following result after some simplification:

$$\begin{aligned}&\sum_{M_g}\langle \alpha_g J_g M_g|[[\mu_4^{(1)}\otimes\mu_j^{(1)}]^{(K)} \\ &\quad\otimes[\mu_2^{(1)}\otimes\mu_i^{(1)}]^{(K)}]_0^{(0)}|\alpha_g J_g M_g\rangle \\ &=(-1)^{K+J_g}(2K+1)^{1/2}\sum_{\alpha J}\sum_{\alpha' J'}\sum_{\alpha'' J''}(-1)^{3J} \\ &\quad\times\begin{Bmatrix} J & J & K \\ 1 & 1 & J'\end{Bmatrix}\begin{Bmatrix} J_g & J_g & K \\ 1 & 1 & J''\end{Bmatrix} \\ &\quad\times\langle \alpha_g J_g\|\mu_4^{(1)}\|\alpha' J'\rangle\langle \alpha' J'\|\mu_j^{(1)}\|\alpha J\rangle \\ &\quad\times\langle \alpha J\|\mu_2^{(1)}\|\alpha'' J''\rangle\langle \alpha'' J''\|\mu_i^{(1)}\|\alpha_g J_g\rangle. \end{aligned}\tag{38}$$

For fully resonant DFWM we have assumed that the excitation bandwidth is sufficiently narrow compared to the density of states (including Doppler broadening) of the absorbing species so that the interaction is exclusively between the degenerate magnetic sublevels of the two levels involved in the one-photon resonant transition. Therefore, the electric dipole operators in Eq. (38) can only connect $\mathbf{J}_g\leftrightarrow\mathbf{J}_e$, i.e., $J''\rightarrow J_e$, $J\rightarrow J_g$, and $J'\rightarrow J_e$, and Eq. (38) simplifies to

$$\begin{aligned}&\sum_{M_g}\langle \alpha_g J_g M_g|[[\mu_4^{(1)}\otimes\mu_j^{(1)}]^{(K)} \\ &\quad\otimes[\mu_2^{(1)}\otimes\mu_i^{(1)}]^{(K)}]_0^{(0)}|\alpha_g J_g M_g\rangle \\ &=(-1)^{K}(2K+1)^{1/2}\begin{Bmatrix} J_g & J_g & K \\ 1 & 1 & J_e\end{Bmatrix}^2 \\ &\quad\times|\langle \alpha_e J_e\|\mu^{(1)}\|\alpha_g J_g\rangle|^4, \end{aligned}\tag{39}$$

where the labels on the electric dipole moment operator have been dropped. The square of the reduced matrix element $\langle \alpha_e J_e\|\mu^{(1)}\|\alpha_g J_g\rangle$ is the molecular line strength $S(\alpha_g J_g;\alpha_e J_e)$ of the $g\leftrightarrow e$ transition, i.e.,

$$\begin{aligned}S(\alpha_g J_g;\alpha_e J_e)&=|\langle \alpha_e J_e\|\mu^{(1)}\|\alpha_g J_g\rangle|^2 \\ &=|\langle \alpha_g J_g\|\mu^{(1)}\|\alpha_e J_e\rangle|^2. \end{aligned}\tag{40}$$

Equation (40) is often expressed[3] as

$$S(\alpha_g J_g;\alpha_e J_e)=S^{\alpha}_{J_g J_e}S^{R}_{J_g J_e},\tag{41}$$

where $S^{\alpha}_{J_g J_e}$ is the strength of the $\alpha_g\leftrightarrow\alpha_e$ vibronic band (in many cases simply the product of the Franck–Condon factor(s) and the square of the electronic transition moment), and $S^{R}_{J_g J_e}$ is the rotational line strength (Hönl–London factor).

Equations (29), (35), and (39) are used to express the key result

$$\begin{aligned}&\sum_{M_g}\langle \alpha_g J_g M_g|\hat{O}|\alpha_g J_g M_g\rangle \\ &=|\langle \alpha_e J_e\|\mu^{(1)}\|\alpha_g J_g\rangle|^4\sum_{K}\begin{Bmatrix} J_g & J_g & K \\ 1 & 1 & J_e\end{Bmatrix}^2 \\ &\quad\times\sum_{Q=-K}^{K}(-1)^{Q}[\epsilon_4^{*(1)}\otimes\epsilon_j^{(1)}]_Q^{(K)}[\epsilon_2^{*(1)}\otimes\epsilon_i^{(1)}]_{-Q}^{(K)}. \end{aligned}\tag{42}$$

The first factor of Eq. (42) represents the dependence of the DFWM signal intensity on the dynamics of the electric dipole interaction, i.e., the greater the line strength of the molecular transition, the larger the DFWM signal intensity. The second factor of Eq. (42) represents the dependence of the DFWM signal intensity on the level degeneracies and the polarization vectors of the electric fields.

The final step in the derivation of the macroscopic polarization is to average over the initial molecular distribution. For an isotropic gas all of the magnetic sublevels of a given level are equally populated ($\rho^{(0)}_{nn}=\rho^{(0)}_{n'n'}$), and no phase relation exists between levels. Therefore the average consists of integrating over the velocity distribution of the absorbing molecules, which is defined as follows:

$$N=\int N(\mathbf{v})d^3v=N\int f(\mathbf{v})d^3v.\tag{43}$$

In most experiments $f(\mathbf{v})$ is the normalized Maxwell-Boltzmann velocity distribution. Using Eqs. (20)–(23), (42), and the identity

$$[T^{(1)}\otimes V^{(1)}]_Q^{(K)}=(-1)^K[V^{(1)}\otimes T^{(1)}]_Q^{(K)},\tag{44}$$

the scalar amplitude of the macroscopic polarization becomes

$$\mathcal{I}^{(3)}_{\mathrm{DFWM}}=\frac{N}{8\hbar^3}(\rho^{(0)}_{gg}-\rho^{(0)}_{ee})|\langle\alpha_e J_e\|\mu^{(1)}\|\alpha_g J_g\rangle|^4\mathscr{E}_1\mathscr{E}_2^*\mathscr{E}_3\Bigg\{\sum_K L^g_{12}(\omega,K)\begin{Bmatrix}J_g & J_g & K\\ 1 & 1 & J_e\end{Bmatrix}^2$$
$$\times\sum_{Q=-K}^{K}(-1)^Q[\epsilon_4^{*(1)}\otimes\epsilon_3^{(1)}]^{(K)}_Q[\epsilon_2^{*(1)}\otimes\epsilon_1^{(1)}]^{(K)}_{-Q}$$
$$+\sum_K L^e_{12}(\omega,K)\begin{Bmatrix}J_e & J_e & K\\ 1 & 1 & J_g\end{Bmatrix}^2\sum_{Q=-K}^{K}(-1)^Q[\epsilon_4^{*(1)}\otimes\epsilon_3^{(1)}]^{(K)}_Q[\epsilon_2^{*(1)}\otimes\epsilon_1^{(1)}]^{(K)}_{-Q}$$
$$+\sum_K L^g_{32}(\omega,K)\begin{Bmatrix}J_g & J_g & K\\ 1 & 1 & J_e\end{Bmatrix}^2\sum_{Q=-K}^{K}(-1)^Q[\epsilon_4^{*(1)}\otimes\epsilon_1^{(1)}]^{(K)}_Q[\epsilon_2^{*(1)}\otimes\epsilon_3^{(1)}]^{(K)}_{-Q}$$
$$+\sum_K L^e_{32}(\omega,K)\begin{Bmatrix}J_e & J_e & K\\ 1 & 1 & J_g\end{Bmatrix}^2\sum_{Q=-K}^{K}(-1)^Q[\epsilon_4^{*(1)}\otimes\epsilon_1^{(1)}]^{(K)}_Q[\epsilon_2^{*(1)}\otimes\epsilon_3^{(1)}]^{(K)}_{-Q}\Bigg\}, \tag{45}$$

where the line shape factors have the form

$$L^n_{j2}(\omega,K)=\int\frac{f(\mathbf{v})d^3v}{[(\mathbf{k}_j-\mathbf{k}_2)\cdot\mathbf{v}-i\Gamma_n(K)]}\left\{\frac{1}{[\omega_0-\omega+\mathbf{k}_j\cdot\mathbf{v}-i\Gamma_{eg}]}-\frac{1}{[\omega_0-\omega+\mathbf{k}_2\cdot\mathbf{v}+i\Gamma_{eg}]}\right\}\frac{1}{[\omega_0-\omega+\mathbf{k}_4\cdot\mathbf{v}-i\Gamma_{eg}]}. \tag{46}$$

In Eq. (45), the $K=0$, 1, and 2 terms describe the (scalar) population, (dipolar) orientation, and (quadupolar) alignment, respectively, and in Eq. (46) the phenomenological relaxation rates $\Gamma_n(K)$ of the spherical tensor representation have replaced the $\Gamma_{n'n}$ rates. The $\Gamma_n(K)$ are defined as follows: $\Gamma_n(0)$ is the relaxation rate of the global population of the nth level, and $\Gamma_n(K=1)$ and $\Gamma_n(K=2)$ are the relaxation rates of the molecular orientation and alignment of the nth level, respectively. Furthermore, we considered only collisional relaxation of the molecular system (no spontaneous emission), and we made the reasonable assumption that for a dipolar transition $\Gamma_{e'g'}=\Gamma_{e'g}=\Gamma_{eg'}=\Gamma_{eg}$, i.e., that only one optical relaxation rate need be considered.[63]

Equation (45) together with Eq. (46) represents the general solution to the DFWM third-order polarization for molecular systems (no hyperfine structure) excited by electric dipole radiation in the weak-field limit and can be evaluated explicitly for the phase matching geometry and polarization configuration of interest. Physically, the third-order DFWM polarization of Eq. (45) is interpreted as resulting from the contributions of four terms: the first term represents the contribution of the diffraction of wave 3 from a ground-state grating formed by fields 1 and 2, the second term represents the contribution of the diffraction of wave 3 from an excited-state grating formed by fields 1 and 2, the third term represents the contribution of the diffraction of wave 1 from a ground-state grating formed by fields 3 and 2, and the fourth term represents the contribution of the diffraction of wave 1 from an excited-state grating formed by fields 3 and 2. In addition the multipole components can be interpreted as ground- and excited-state population, orientation, alignment gratings for $K=0$, 1, and 2, respectively. This treatment demonstrates that in the most general case the DFWM signal may be regarded as arising from the contributions of twelve different gratings! The gratings can be distinguished by spacing ($\Delta\mathbf{k}_{12}$ or $\Delta\mathbf{k}_{32}$), by the level in which the grating is formed (ground or excited), and by the multipole nature of the grating (population, orientation, or alignment).

To complete our derivation, Eq. (45) is substituted into Eq. (19) to yield the expression[64] for the DFWM signal intensity

$$I_{\mathrm{DFWM}}\propto\left[N_g-\frac{(2J_g+1)}{(2J_e+1)}N_e\right]^2[B_{ge}(J_g,J_e)]^4I_1I_2I_3$$
$$\times\Bigg|\sum_K L^g_{12}(\omega,K)G(J_g,J_e;K)F(\epsilon_4,\epsilon_1,\epsilon_3,\epsilon_2;K)$$
$$+\sum_K L^e_{12}(\omega,K)G(J_e,J_g;K)F(\epsilon_4,\epsilon_1,\epsilon_3,\epsilon_2;K)$$
$$+\sum_K L^g_{32}(\omega,K)G(J_g,J_e;K)F(\epsilon_4,\epsilon_3,\epsilon_1,\epsilon_2;K)$$
$$+\sum_K L^e_{32}(\omega,K)G(J_e,J_g;K)F(\epsilon_4,\epsilon_3,\epsilon_1,\epsilon_2;K)\Bigg|^2, \tag{47}$$

where the following substitutions have been made:

$$N_g-\frac{(2J_g+1)}{(2J_e+1)}N_e=N(2J_g+1)(\rho^{(0)}_{gg}-\rho^{(0)}_{ee}), \tag{48}$$

$$[B_{ge}(J_g,J_e)]^2=\left[\frac{\pi}{3\epsilon_0\hbar^2}\right]^2\frac{|\langle\alpha_e J_e\|\mu^{(1)}\|\alpha_g J_g\rangle|^4}{(2J_g+1)^2}, \tag{49}$$

$$G(J,J';K)=(2J_g+1)\begin{Bmatrix}J & J & K\\ 1 & 1 & J'\end{Bmatrix}^2, \tag{50}$$

and

TABLE IV. Analytic expressions for $G(J,J',K) = (2J_g + 1)\{^{J\,J\,K}_{1\,1\,J'}\}^2$ as a function of transition type and K value.

$J'-J$	$G(J,J';0)$	$G(J,J';1)$	$G(J,J';2)$
-1	$\frac{1}{3}\left[\frac{2J_g+1}{2J+1}\right]$	$\frac{1}{6}\left[\frac{J+1}{J}\right]\left[\frac{2J_g+1}{2J+1}\right]$	$\frac{1}{30}\left[\frac{(2J+3)(J+1)}{J(2J-1)}\right]\left[\frac{2J_g+1}{2J+1}\right]$
0	$\frac{1}{3}\left[\frac{2J_g+1}{2J+1}\right]$	$\frac{1}{6}\left[\frac{1}{J(J+1)}\right]\left[\frac{2J_g+1}{2J+1}\right]$	$\frac{1}{30}\left[\frac{(2J+3)(2J-1)}{J(J+1)}\right]\left[\frac{2J_g+1}{2J+1}\right]$
$+1$	$\frac{1}{3}\left[\frac{2J_g+1}{2J+1}\right]$	$\frac{1}{6}\left[\frac{J}{J+1}\right]\left[\frac{2J_g+1}{2J+1}\right]$	$\frac{1}{30}\left[\frac{J(2J-1)}{(2J+3)(J+1)}\right]\left[\frac{2J_g+1}{2J+1}\right]$

$$F(\boldsymbol{\epsilon}_4,\boldsymbol{\epsilon}_i,\boldsymbol{\epsilon}_j,\boldsymbol{\epsilon}_2;K)=\sum_{Q=-K}^{K}(-1)^Q[\boldsymbol{\epsilon}_4^{*(1)}\otimes\boldsymbol{\epsilon}_j^{(1)}]_Q^{(K)}\times[\boldsymbol{\epsilon}_2^{*(1)}\otimes\boldsymbol{\epsilon}_i^{(1)}]_{-Q}^{(K)}. \tag{51}$$

In Eq. (50) the $G(J,J',K)$ factors are simply 6-j symbols and depend only on K, J_g, and J_e. These values are listed in Table IV as a function of transition type. Conversely, the $F(\boldsymbol{\epsilon}_4,\boldsymbol{\epsilon}_i,\boldsymbol{\epsilon}_j,\boldsymbol{\epsilon}_2;K)$ factors of Eq. (51) depend on the field polarizations but not on J_g and J_e. The polarization tensor products of Eq. (51) are evaluated in the Appendix, and the results for specific polarization cases treated in Sec. II are given in Table V.

B. Equal relaxation of the multipole moments

In Sec. II we assumed that the relaxation is isotropic and that all of the state multipoles relax at the same rate. For many experiments, population relaxation rates such as quenching are much larger than collisional rates that only perturb the magnetic sublevel distribution. Therefore, a single relaxation rate might be expected to characterize the nth level. Some experimental evidence supports this "single relaxation" assumption.[17,65]

Under the "single relaxation" assumption the line shape factors of Eq. (46) become K independent and take the form of Eq. (7) of Sec. II A, i.e., $L_{j2}^n(\omega,K)\rightarrow L_{j2}^n(\omega)$. Removing the line shape factors from the summations of Eq. (47) gives the familiar expression of Eq. (2) with the total geometric factor $G_F^T(\boldsymbol{\epsilon}_4,\boldsymbol{\epsilon}_1,\boldsymbol{\epsilon}_3,\boldsymbol{\epsilon}_2;J_g,J_e;\omega)$ defined in terms of an expansion in K as

TABLE V. Analytic expressions for $F(\boldsymbol{\epsilon}_4,\boldsymbol{\epsilon}_i,\boldsymbol{\epsilon}_j,\boldsymbol{\epsilon}_2;K) = \Sigma_{Q=-K}^{K}(-1)^Q[\boldsymbol{\epsilon}_4^{*(1)}\otimes\boldsymbol{\epsilon}_j^{(1)}]_Q^{(K)}[\boldsymbol{\epsilon}_2^{*(1)}\otimes\boldsymbol{\epsilon}_i^{(1)}]_{-Q}^{(K)}$ as a function of polarization configuration and K value.

$\boldsymbol{\epsilon}_4\boldsymbol{\epsilon}_i\boldsymbol{\epsilon}_j\boldsymbol{\epsilon}_2$	$F(\boldsymbol{\epsilon}_4,\boldsymbol{\epsilon}_i,\boldsymbol{\epsilon}_j,\boldsymbol{\epsilon}_2;0)$	$F(\boldsymbol{\epsilon}_4,\boldsymbol{\epsilon}_i,\boldsymbol{\epsilon}_j,\boldsymbol{\epsilon}_2;1)$	$F(\boldsymbol{\epsilon}_4,\boldsymbol{\epsilon}_i,\boldsymbol{\epsilon}_j,\boldsymbol{\epsilon}_2;2)$
RRRR	1/3	1/2	1/6
RLRL	1/3	−1/2	1/6
RRLL	0	0	1
YYYY	1/3	0	2/3
YXYX	1/3	0	−1/3
YYXX	0	1/2	1/2
YXXY	0	−1/2	1/2

$$\begin{aligned}G_F^T(\boldsymbol{\epsilon}_4,\boldsymbol{\epsilon}_1,\boldsymbol{\epsilon}_3,\boldsymbol{\epsilon}_2;J_g,J_e;\omega)&=\frac{1}{\mathscr{L}(\omega)}\Bigg\{L_{12}^g(\omega)\sum_K G(J_g,J_e;K)F(\boldsymbol{\epsilon}_4,\boldsymbol{\epsilon}_1,\boldsymbol{\epsilon}_3,\boldsymbol{\epsilon}_2;K)\\&+L_{12}^e(\omega)\sum_K G(J_e,J_g;K)F(\boldsymbol{\epsilon}_4,\boldsymbol{\epsilon}_1,\boldsymbol{\epsilon}_3,\boldsymbol{\epsilon}_2;K)\\&+L_{32}^g(\omega)\sum_K G(J_g,J_e;K)F(\boldsymbol{\epsilon}_4,\boldsymbol{\epsilon}_3,\boldsymbol{\epsilon}_1,\boldsymbol{\epsilon}_2;K)\\&+L_{32}^e(\omega)\sum_K G(J_e,J_g;K)F(\boldsymbol{\epsilon}_4,\boldsymbol{\epsilon}_3,\boldsymbol{\epsilon}_1,\boldsymbol{\epsilon}_2;K)\Bigg\}\\&=\sum_K G_F^{T(K)}(\boldsymbol{\epsilon}_4,\boldsymbol{\epsilon}_1,\boldsymbol{\epsilon}_3,\boldsymbol{\epsilon}_2;J_g,J_e;\omega),\end{aligned} \tag{52}$$

where the dependence of the line shape factors on collisions and phase matching is the same as in Sec. II. Equation (52) reduces to Eq. (4) of Sec. II A because

$$\begin{aligned}\sum_K\begin{Bmatrix}J&J&K\\1&1&J'\end{Bmatrix}^2\sum_{Q=-K}^{K}(-1)^Q[\boldsymbol{\epsilon}_4^{*(1)}\otimes\boldsymbol{\epsilon}_j^{(1)}]_Q^{(K)}\times[\boldsymbol{\epsilon}_2^{*(1)}\otimes\boldsymbol{\epsilon}_i^{(1)}]_{-Q}^{(K)}\\=\sum_K\begin{Bmatrix}J'&J'&K\\1&1&J\end{Bmatrix}^2\sum_{Q=-K}^{K}(-1)^Q[\boldsymbol{\epsilon}_4^{*(1)}\otimes\boldsymbol{\epsilon}_i^{(1)}]_Q^{(K)}\times[\boldsymbol{\epsilon}_2^{*(1)}\otimes\boldsymbol{\epsilon}_j^{(1)}]_{-Q}^{(K)}.\end{aligned} \tag{53}$$

This identity is proven in Appendix A of Ref. 30. Equation (53) results from the fact the first four-photon matrix element product in Eq. (22) differs from the second product only in the ordering of the matrix elements. Because each matrix element is simply a complex number, it is immediately obvious that

$$\begin{aligned}\sum_{\text{all }M}\langle g|\boldsymbol{\epsilon}_4^*\cdot\boldsymbol{\mu}|e'\rangle\langle e'|\boldsymbol{\epsilon}_j\cdot\boldsymbol{\mu}|g'\rangle\langle g'|\boldsymbol{\epsilon}_2^*\cdot\boldsymbol{\mu}|e\rangle\langle e|\boldsymbol{\epsilon}_i\cdot\boldsymbol{\mu}|g\rangle\\=\sum_{\text{all }M}\langle e'|\boldsymbol{\epsilon}_j\cdot\boldsymbol{\mu}|g'\rangle\langle g'|\boldsymbol{\epsilon}_2^*\cdot\boldsymbol{\mu}|e\rangle\langle e|\boldsymbol{\epsilon}_i\cdot\boldsymbol{\mu}|g\rangle\\\times\langle g|\boldsymbol{\epsilon}_4^*\cdot\boldsymbol{\mu}|e'\rangle.\end{aligned} \tag{54}$$

Note, however, that the ordering of the angular momentum coupling is different for the two four-photon matrix element products of Eq. (54). From Eqs. (4), (52), and (53), the geometric factors are defined as

$$\begin{aligned}G_F(\boldsymbol{\epsilon}_4,\boldsymbol{\epsilon}_i,\boldsymbol{\epsilon}_j,\boldsymbol{\epsilon}_2;J_g,J_e)&=\sum_K G(J_g,J_e;K)F(\boldsymbol{\epsilon}_4,\boldsymbol{\epsilon}_i,\boldsymbol{\epsilon}_j,\boldsymbol{\epsilon}_2;K)\\&=\sum_K G(J_e,J_g;K)F(\boldsymbol{\epsilon}_4,\boldsymbol{\epsilon}_j,\boldsymbol{\epsilon}_i,\boldsymbol{\epsilon}_2;K).\end{aligned} \tag{55}$$

Equation (55) was used to generate the results found in Tables I–III.

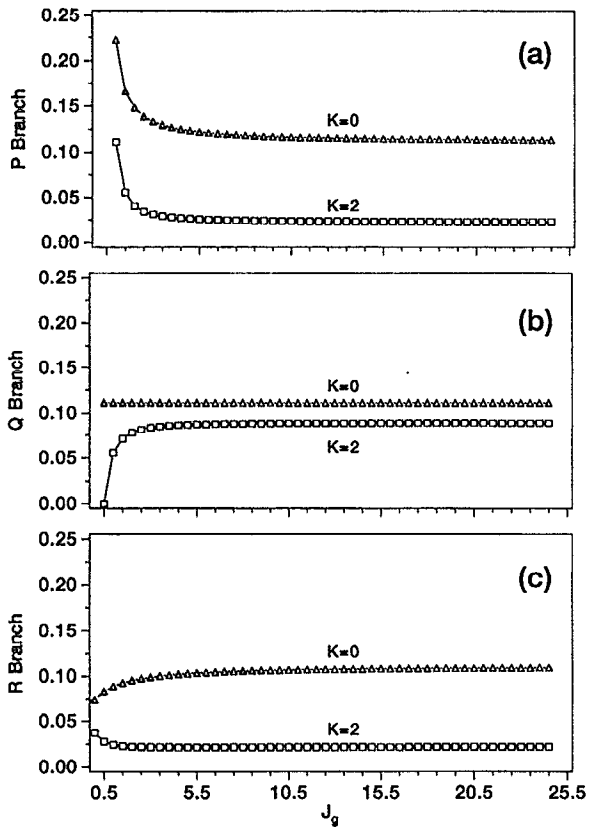

FIG. 5. Evaluated $G_F^{T(K)}(Y,Y,Y,Y;J_g,J_e;\omega)$ factors as a function of J_g for (a) P-branch, (b) Q-branch, and (c) R-branch transitions. Permuting $X \leftrightarrow Y$ does not change the plots. In the figure -△- and -□- correspond to $K=0$ and 2, respectively.

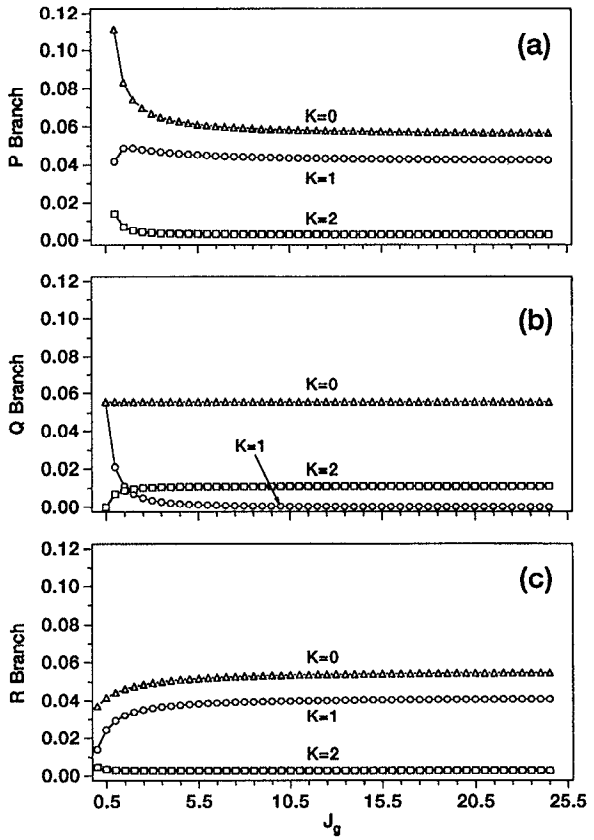

FIG. 6. Evaluated $G_F^{T(K)}(Y,X,Y,X;J_g,J_e;\omega) = G_F^{T(K)}(Y,Y,X,X;J_g,J_e;\omega) = \frac{1}{2}G_F^{T(K)}(R,R,R,R;J_g,J_e;\omega)$ factors as a function of J_g for (a) P-branch, (b) Q-branch, and (c) R-branch transitions. Permuting $X \leftrightarrow Y$ or $R \leftrightarrow L$ does not change the plots. In the figure -△-, -○-, and -□- correspond to $K=0$, 1, and 2, respectively.

The geometric factor $G_F^{T(K)}(\epsilon_4,\epsilon_1,\epsilon_3,\epsilon_2;J_g,J_e;\omega)$ of Eq. (52) is interpreted as being proportional to the total contribution of the 2^K multipole moment of the total angular momentum distribution to the DFWM signal amplitude along ϵ_4. We have plotted the $G_F^{T(K)}(\epsilon_4,\epsilon_1,\epsilon_3,\epsilon_2;J_g,J_e;\omega)$ for experimental conditions where $L_{12}^n(\omega)=L_{32}^n(\omega)$ and the upper and lower levels relax at the same rate, i.e., for the cases where the total geometric factor is decoupled from the collisional effects and phase matching geometry of the experiment. These results are shown in Figs. 5–8. Note that inherent in Eq. (52) is the assumption that the relaxation is isotropic and all of the state multipoles relax at the same rate. The conditions that Figs. 5–8 describe are very specific; however, the discussion presented below can be extended to most experiments.

Figures 5 and 6 show the $G_F^{T(K)}(\epsilon_4,\epsilon_1,\epsilon_3,\epsilon_2;J_g,J_e;\omega)$ values as a function of J_g when the fields have identical polarizations, either linear (X or Y) or circular (R or L). According to the grating picture, interference of the grating-forming fields produces a spatial modulation of laser intensity with spacing given by Eq. (11). These intensity gratings are usually referred to as population gratings, but as can be seen in Figs. 5 and 6, the DFWM signal amplitude has significant contributions from higher-order moments. For instance, the population and alignment contributions to the DFWM signal amplitude for a Q-branch transition excited with linear polarized light [see Fig. 5(b)] are nearly equal! This and other effects can be understood by employing known concepts from linear spectroscopy to develop a qualitative picture of DFWM.

The first step is to recognize that, although the intensity is spatially modulated, the field polarization in these regions is preserved. Thus we can think of the initial isotropic distribution of absorbers interacting with polarized light in spatially distinct regions. For linearly polarized light, we would expect to create a spatial modulation of the population and alignment of the absorbers, i.e., population and alignment gratings. As shown in Fig. 5, only population and alignment gratings contribute. Likewise for circularly polarized light, we would expect to create a spatial modulation of the population, orientation, and alignment of the absorbers, i.e., population, orientation, and alignment gratings. Figure 6 shows that this expectation is indeed met.

Another interesting case involves linear polarized light in which both pump fields have the same polarization but are orthogonally polarized with respect to the probe field (see Fig. 7). The interference produced in this case is spatially uniform in intensity but spatially modulated in polarization. This polarization grating is typically referred to as a coher-

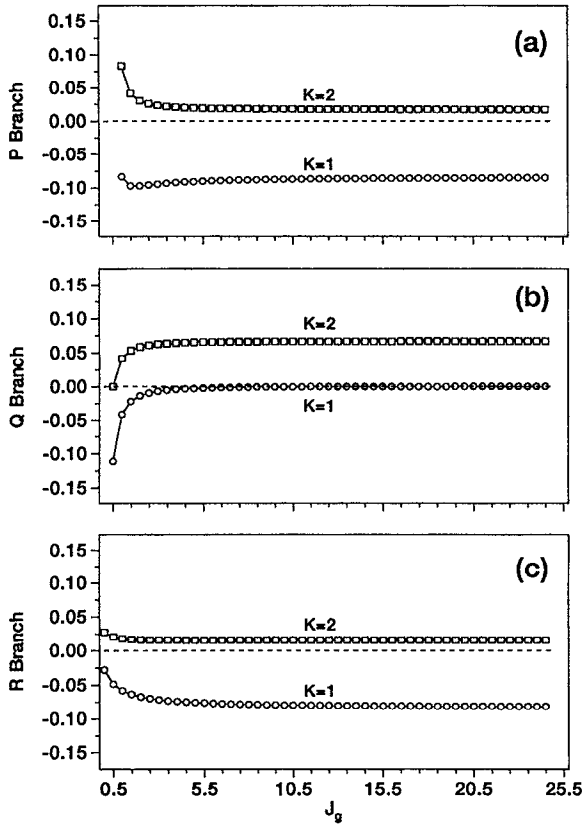

FIG. 7. Evaluated $G_F^{T(K)}(Y,X,X,Y;J_g,J_e;\omega)$ factors as a function of J_g for (a) P-branch, (b) Q-branch, and (c) R-branch transitions. Permuting $X \leftrightarrow Y$ does not change the plots. In the figure -○-, and -□- correspond to $K=1$ and 2, respectively.

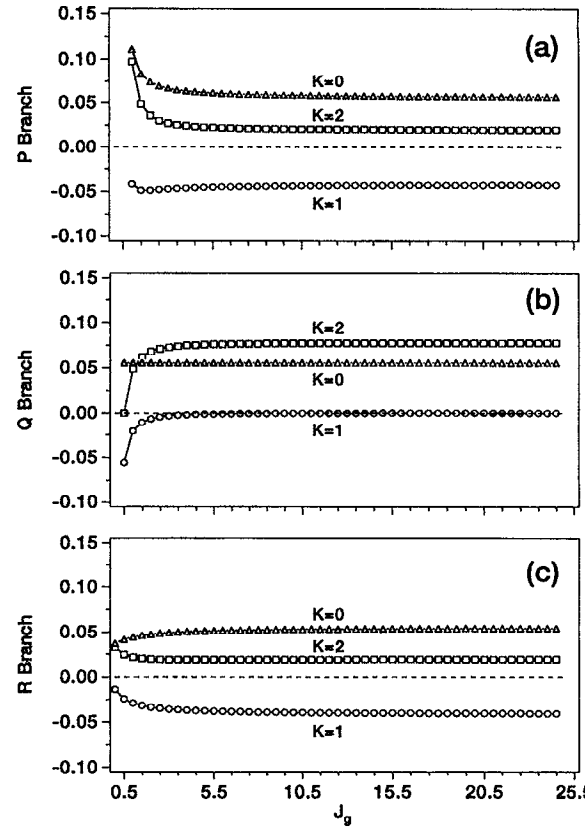

FIG. 8. Evaluated $G_F^{T(K)}(R,L,R,L;J_g,J_e;\omega)=G_F^{T(K)}(R,R,L,L;J_g,J_e;\omega)$ factors as a function of J_g for (a) P-branch, (b) Q-branch, and (c) R-branch transitions. Permuting $R \leftrightarrow L$ does not change the plots. In the figure -△-, -○-, and -□- correspond to $K=0$, 1, and 2, respectively.

ence grating because spatial population modulation does not exist. Under these circumstances only orientation and alignment contributions are expected, as confirmed in Fig. 7.

In Fig. 7 orientation gratings are found to dominate for $\Delta J=\pm 1$ transitions and alignment gratings dominate for $\Delta J=0$ transitions. Furthermore, inspection of Figs. 6–8 shows that this conclusion is generally true. This behavior can be understood, again, if we consider the interaction of an isotropic distribution of molecules interacting with polarized light. After the absorption of linearly polarized light the system will be aligned, and after the absorption of circularly polarized light the system will be oriented and aligned. Q-branch transitions are more easily aligned than oriented, and the opposite is true for P- and R-branch transitions.

Finally, the most significant aspect of Figs. 5–8 is that the relative multipole moment contributions are very dependent on the value of J for low J values, but rapidly approach a high-J limit, i.e., for $J \geqslant 4$ the total geometric factor and its relative contributions are essentially independent of J. This behavior means that the J dependence of the DFWM signal intensity for a given branch (P, Q, or R) taken in a single polarization configuration will primarily reflect the J dependence of the one-photon absorption coefficient B_{ge} as well as any J-dependent relaxation effects. Molecules are often in the high-J limit, especially at flame and plasma temperatures at which J values ranging from 5 to 50 are typically populated.

C. Unequal relaxation of the multipole moments

We have assumed thus far that the multipole moments relax at equal rates, which is a good approximation in flame experiments where efficient energy transfer collision partners, such as water, are present. We have recently observed[65] experimental conditions for which these rates are not the same, particularly for low values of **J**, in collisional environments in which light species such as helium are the dominant collision partners. Such species have slow inelastic collisional rates (quenching) compared with elastic collisional rates (disorienting). The presence of unequal relaxation can be determined by polarization-ratio measurements.[17,65]

In the event that the multipole moments of the angular momentum distribution do not relax equally, the expressions for the DFWM signal intensity presented in Sec. II do not apply. If the relaxation is isotropic, however, the multipole moments relax independently, and the expressions presented in Sec. III A are valid. The effects of unequal relaxation has been discussed by Ducloy and Bloch[30] and is the topic of a future publication.[65] Finally, if the relaxation is anisotropic, for example, the gas is in a static electric or magnetic field,

then the situation is considerably more complicated.[34,56] Note, however, that the interpretation of DFWM signal intensities at this level of detail is not necessary for most applications.

IV. COMPARISON WITH PREVIOUS WORK

In what follows we attempt to place our work in the context of previous perturbative theoretical treatments of DFWM. Lam and Abrams (LA)[29] were among the first to describe the polarization effects for a degenerate two-level system. They used a density matrix approach to express the DFWM response as a summation of matrix element products that represented different coherences corresponding to contributions from normal population, cross-population, and Zeeman coherence mechanisms. Although this model provides an intuitive picture for the origin of the DFWM polarization effects, its application depends on the coordinate system chosen. This coordinate-frame dependence also makes the inclusion of collisional relaxation difficult, and LA acknowledged that an accurate description of the DFWM collisional effects in systems with degenerate sublevels necessitates the introduction of the irreducible (spherical tensor) representation of the density matrix.[56,57]

Such an approach was presented by Ducloy and Bloch (DB),[30] who discussed the DFWM response in terms of its irreducible tensor components. In their tensorial density matrix treatment, DB considered the degeneracy of the resonant levels, unequal relaxation of the magnetic sublevels, spontaneous emission (optical pumping), thermal motion, and the effect of pump–probe angular separation (noncollinear geometries). In later papers Berman, Steel, Khitrova, and Liu (BSKL)[31] and Alekseev[35] derived similar expressions that also included the effects of hyperfine structure. Together the work of DB, BSKL, and Alekseev illustrates the fundamental aspects of DFWM in the perturbative regime and represents general solutions of the problem. Unfortunately these studies have not been available to most experimentalists because the final results, expressed in density matrix notation, are quite complicated. Recently Kupiszewska and Whitaker (KW)[38] addressed this problem by specializing the treatment of BSKL to stationary diatomic molecules described by Hund's case (a) coupling with no hyperfine structure. The simplified expressions presented by KW provide some insight into the polarization effects in DFWM for molecular systems; however, the specialization of the treatment necessarily limits the applicability of the results.

An alternative approach to interpret DFWM signal intensities is to use diagrammatic perturbation theory (double-sided Feynman diagrams) to evaluate the DFWM polarization and collisional effects.[40,41,58] The diagrammatic method is equivalent to the density matrix formalism but has the advantage that the third-order nonlinear polarization can be evaluated directly without the need to calculate lower-order processes. Using diagrammatic methods, Attal-Trétout, Monot, and Müller-Dethlefs (TMD)[33] and Aben, Ubachs, van der Zwan, and Hogervorst (AUZH)[36] have derived expressions for resonant CARS spectroscopy. This work focused on obtaining four-wave mixing line strength factors for diatomic molecules (omitting nuclear spin) to be used directly in the analysis of experimental signal intensities. Both TMD and AUZH note that the CARS expressions could be extended to describe DFWM, i.e., fully resonant CARS. We noted in Sec. II that the line strength factors themselves are dependent on the relaxation caused by the environment and not just angular momentum considerations. Consequently, this suggestion is correct only with qualification.

The general CARS expressions involve four distinct frequencies ω_1, ω_2, ω_3, and ω_4, and four independent states $|a\rangle$, $|b\rangle$, $|c\rangle$, $|d\rangle$ (labeled a, n, b, n' in TMD and a, b, c, d in AUZH). In the fully resonant case, $\omega_1=\omega_2=\omega_3=\omega_4=\omega$, and the four independent states converge to four distinct magnetic sublevels, i.e., $|a\rangle\rightarrow|g\rangle$, $|b\rangle\rightarrow|e\rangle$, $|c\rangle\rightarrow|g'\rangle$, and $|d\rangle=|e'\rangle$. This mapping leads to the inclusion of eight diagrams (eight more if $N_e\neq 0$) and four distinct resonant four-photon matrix element products, namely,

$$\sum_{\text{all } M}\langle g|\boldsymbol{\epsilon}_4^*\cdot\boldsymbol{\mu}|e'\rangle\langle e'|\boldsymbol{\epsilon}_3\cdot\boldsymbol{\mu}|g'\rangle\langle g'|\boldsymbol{\epsilon}_2^*\cdot\boldsymbol{\mu}|e\rangle\langle e|\boldsymbol{\epsilon}_1\cdot\boldsymbol{\mu}|g\rangle, \tag{56a}$$

$$\sum_{\text{all } M}\langle e'|\boldsymbol{\epsilon}_3\cdot\boldsymbol{\mu}|g'\rangle\langle g'|\boldsymbol{\epsilon}_2^*\cdot\boldsymbol{\mu}|e\rangle\langle e|\boldsymbol{\epsilon}_1\cdot\boldsymbol{\mu}|g\rangle\langle g|\boldsymbol{\epsilon}_4^*\cdot\boldsymbol{\mu}|e'\rangle, \tag{56b}$$

$$\sum_{\text{all } M}\langle g|\boldsymbol{\epsilon}_4^*\cdot\boldsymbol{\mu}|e'\rangle\langle e'|\boldsymbol{\epsilon}_1\cdot\boldsymbol{\mu}|g'\rangle\langle g'|\boldsymbol{\epsilon}_2^*\cdot\boldsymbol{\mu}|e\rangle\langle e|\boldsymbol{\epsilon}_3\cdot\boldsymbol{\mu}|g\rangle, \tag{56c}$$

and

$$\sum_{\text{all } M}\langle e'|\boldsymbol{\epsilon}_1\cdot\boldsymbol{\mu}|g'\rangle\langle g'|\boldsymbol{\epsilon}_2^*\cdot\boldsymbol{\mu}|e\rangle\langle e|\boldsymbol{\epsilon}_3\cdot\boldsymbol{\mu}|g\rangle\langle g|\boldsymbol{\epsilon}_4^*\cdot\boldsymbol{\mu}|e'\rangle. \tag{56d}$$

Equations (56a) and (56b) have the same value when summed over all M, but the ordering of the angular momentum coupling is different, and thus they represent different contributions from the zeroth, first, and second rank multipole moments. The same is true for Eqs. (56c) and (56d). The proper accounting of the multipole moment contributions, to our knowledge, has not been done using diagrammatic perturbation theory but has been done using density matrix approaches.[30,31,38] In addition Eqs. (56a) and (56c) appear quite similar, but have distinctly different values even when summed over all M, and the same is true for Eqs. (56b) and (56d). Therefore care must be taken in extending CARS expressions to DFWM.

Bervas, Le Boiteux, Labrunie, Attal-Trétout (BBLT)[37] and Freidman-Hill, Rahn, and Farrow (HRF)[39] recently reduced the CARS expressions to apply to DFWM. The expressions of BBLT contradict our results for BB- and PC-DFWM but agree fortuitously with our results for FB-DFWM. We offer the following explanation for these results. In Fig. 4 of BBLT, diagrams (a)–(d) describe the primary contributions to BB- and, PC-DFWM in the Doppler-broadened limit, and diagrams (a)–(h) describe the primarily contributions to FB-DFWM. Because BBLT do not distinguish between g and g' or e and e', all of the diagrams appear to be represented by the same matrix element prod-

uct, namely Eq. (8) of BBLT. Diagrams (a) and (c) of BBLT Fig. 4 correspond to our Eq. (56a), diagrams (b) and (d) of BBLT Fig. 4 correspond to our Eq. (56d), diagrams (e) and (g) of BBLT Fig. 4 correspond to our Eq. (56c), and diagrams (f) and (h) of BBLT Fig. 4 correspond to our Eq. (56b). In terms of the notation developed in this paper, the result of BBLT predicts the following proportionality for the BB- and PC-DFWM signal intensity:

$$I_{\mathrm{BB,PC}} \propto |G_F(\epsilon_4,\epsilon_1,\epsilon_3,\epsilon_2;J_g,J_e)[L^g_{12}(\omega)+L^e_{12}(\omega)]|^2, \tag{57a}$$

which is independent of the difference in the relaxation rates of the g and e levels for all polarization configurations, whereas our treatment predicts that

$$I_{\mathrm{BB,PC}} \propto |G_F(\epsilon_4,\epsilon_1,\epsilon_3,\epsilon_2;J_g,J_e)L^g_{12}(\omega) + G_F(\epsilon_4,\epsilon_3,\epsilon_1,\epsilon_2;J_g,J_e)L^e_{12}(\omega)|^2, \tag{57b}$$

which is dependent on the relative relaxation rates of the g and e levels whenever the two geometric factors differ (see Sec. II). Furthermore, our result, Eq. (57b), agrees with Eq. (45) of DB derived using a density matrix approach and experimental DFWM polarization ratios obtained in our laboratory for the CH radical.[17] The expressions for FB-DFWM presented by BBLT agree with our results because $L^g_{12}(\omega)=L^g_{32}(\omega)$ and $L^e_{12}(\omega)=L^e_{32}(\omega)$. In our notation, BBLT predict the following proportionality for the FB-DFWM signal intensity:

$$I_{\mathrm{FB}} \propto |G_F(\epsilon_4,\epsilon_1,\epsilon_3,\epsilon_2;J_g,J_e)[L^g_{12}(\omega)+L^e_{12}(\omega)] + G_F(\epsilon_4,\epsilon_3,\epsilon_1,\epsilon_2;J_g,J_e)[L^g_{32}(\omega)+L^e_{32}(\omega)]|^2, \tag{58a}$$

which is equivalent to our result

$$I_{\mathrm{FB}} \propto |G_F(\epsilon_4,\epsilon_1,\epsilon_3,\epsilon_2;J_g,J_e)[L^g_{12}(\omega)+L^e_{32}(\omega)] + G_F(\epsilon_4,\epsilon_3,\epsilon_1,\epsilon_2;J_g,J_e)[L^e_{12}(\omega)+L^g_{32}(\omega)]|^2, \tag{58b}$$

when $L^g_{12}(\omega)=L^g_{32}(\omega)$ and $L^e_{12}(\omega)=L^e_{32}(\omega)$. HRF considered three-level or "crossover" resonances that occur when two transitions that share a common level become resonant because of a simultaneous Doppler shift. HRF show that crossover resonances can influence DFWM signal intensities even if they are not spectroscopically resolved from their parent transitions. Such considerations could be important in spectrally congested regions with overlapping branches.

In summary, the work to date can be classified in two categories: first, density matrix approaches that emphasize the complex relation between polarization, collisional relaxation, and phase matching at the expense of simplicity; and second, diagrammatic approaches that focus on expressing the polarization effects (without specifying multipole contributions) analytically while treating relaxation effects superficially. The emphasis of this paper has been on the key aspects of interpreting molecular DFWM spectra in collisionally dominated environments because these types of experiments are those for which DFWM has found the largest application. In these experiments, hyperfine structure, spontaneous emission, and in most circumstances unequal relaxation of the multipole moments of the angular momentum distribution can be neglected so that relatively simple expressions are obtained without unnecessarily trivializing the treatment. Thus we have attempted to combine the best aspects of the two approaches by presenting analytic expressions with the relevant collision, velocity, and polarization considerations for the most-utilized experimental configurations. These expressions can be used directly in the evaluation of DFWM spectra for these specific cases. Finally, the polarization tensor products evaluated in the Appendix can be used to extend the general expressions of Sec. III A to other experimental geometries of interest.

The above results were derived in the weak-field (no saturation) limit. An appealing aspect of DFWM is that in the saturation regime, the DFWM signal intensity becomes relatively insensitive to the specific value of the relaxation rates.[11,28] In this regime, the problem of extracting relative population distributions essentially reduces to knowing the absorption coefficients. This aspect is discussed in detail in WZR2.

V. CONCLUSIONS

In the present paper we derived expressions via time-independent diagrammatic perturbation theory that account for the DFWM polarization, collisional, and velocity effects in the weak-field limit (no saturation). In our treatment, we assumed that the DFWM process couples levels of sharp (definite) angular momentum **J**. Three input fields of arbitrary polarization interact with an isotropic sample to produce a fourth field. The general result (Sec. III) was specialized to apply to circularly and linearly polarized fields that interact in nearly collinear phase matching geometries in collisional environments where the multipole moments of the total angular momentum distribution relax independently (isotropic relaxation) and at the same rate. These specialized expressions (Sec. II) generally apply to DFWM experiments performed in collisionally dominated environments.

In Sec. II we showed that the DFWM signal intensity for collisionally dominated systems is proportional to the square of the concentration difference of the levels involved in the one-photon resonant transition, the fourth power of the one-photon transition strength, the square of a total line shape function, and the square of the total geometric factor. The total geometric factor was shown to depend not only on the polarization of the input fields but also on the specifics of the experiment, i.e., collisional relaxation, velocity, and phase matching. This interdependence complicated the interpretation of the DFWM polarization response but also enabled qualitative information about the collisional relaxation caused by the environment to be obtained from polarization measurements.

Finally in Sec. III, we showed that in the most general case the DFWM signal may be regarded as arising from the contributions of 12 different gratings. These gratings are distinguished by spacing ($\Delta\mathbf{k}_{12}$ or $\Delta\mathbf{k}_{32}$), by the level in which the grating is formed (ground or excited), and by the multipole nature of the grating (population, orientation, or alignment). Therefore, simple population vs coherence grating

pictures of DFWM are not adequate descriptions. For instance, DFWM experiments in which all fields are the same polarization (either linear or circular) have contributions (in addition to population) from higher-order moments of the total angular momentum distribution, namely, alignment for linear, and orientation and alignment for circular. We also showed that the relative multipole moment contributions depend strongly on J for low J values but rapidly approach a high-J limit. In this limit the J dependence of the DFWM signal intensity for a given branch (P, Q, or R) taken with a single polarization configuration primarily reflects the J dependence of the one-photon absorption coefficient B_{ge} as well as any J-dependent relaxation effects.

We have discussed the key aspects of DFWM in reference to molecular species in collisionally dominated environments. We presented explicit expressions for the DFWM signal intensity that can be used with molecular absorption and relaxation data to obtain the relative population distributions. Absorption data in the form of cross sections, line strengths, emission coefficients, etc., are available for most molecules of interest. However, obtaining an accurate and complete set of relaxation rates for a given molecule in a specific environment is a formidable task.

ACKNOWLEDGMENTS

The authors are grateful to A. J. Orr-Ewing, R. Trebino, and B. J. Whittaker for helpful comments. S. Williams thanks the Air Force Office of Scientific Research for an AFOSR Graduate Fellowship and the Department of Energy for a AWU-DOE Graduate Fellowship. This work was supported by the Air Force Office of Scientific Research (F49620-92-J-0074) and the U.S. Department of Energy, Office of Basic Energy Sciences, Division of Chemical Sciences.

APPENDIX: CALCULATION OF THE POLARIZATION TENSOR PRODUCTS

In this Appendix we establish the notation used for expressing the polarization unit vectors and evaluate the polarization tensor products necessary to calculate the DFWM signal intensity for experimental configurations not treated in the text. In what follows, we rely on the definitions of symbols already introduced.

An arbitrary vector $\mathbf{r}$ can be expressed in Cartesian coordinates as

$$\mathbf{r}=r_x\mathbf{e}_x+r_y\mathbf{e}_y+r_z\mathbf{e}_z, \tag{A1}$$

and its complex conjugate $\mathbf{r}^*$ as

$$\mathbf{r}^*=r_x^*\mathbf{e}_x+r_y^*\mathbf{e}_y+r_z^*\mathbf{e}_z, \tag{A2}$$

where $\mathbf{e}_x$, $\mathbf{e}_y$, and $\mathbf{e}_z$ are unit vectors and r_x, r_y, and r_z are the standard Cartesian components of the vector $\mathbf{r}$. The conventions for relating the unit vectors and the standard components of the Cartesian (real) basis to the spherical tensor (complex) basis are defined as follows:

$$\mathbf{e}_{\pm1}=\mp\frac{1}{\sqrt{2}}(\mathbf{e}_x\pm i\mathbf{e}_y),\quad \mathbf{e}_0=\mathbf{e}_z, \tag{A3}$$

and

$$r_{\pm1}^{(1)}=\mp\frac{1}{\sqrt{2}}(r_x\pm ir_y),\quad r_0^{(1)}=r_z. \tag{A4}$$

It follows that

$$\mathbf{e}_q^*=(-1)^q\mathbf{e}_{-q},\quad \mathbf{e}_q\cdot\mathbf{e}_{q'}^*=\delta_{qq'}, \tag{A5}$$

and

$$(r^*)_q^{(1)}=(-1)^q[r_{-q}^{(1)}]^* \tag{A6}$$

where $q=0,\pm1$. Equations (A3) and (A4) in turn define the conventions for relating the unit vectors and the standard components of the spherical tensor basis to the Cartesian basis, i.e.,

$$\mathbf{e}_x=-\frac{1}{\sqrt{2}}(\mathbf{e}_{+1}-\mathbf{e}_{-1}),\quad \mathbf{e}_y=\frac{i}{\sqrt{2}}(\mathbf{e}_{+1}+\mathbf{e}_{-1}),\quad \mathbf{e}_z=\mathbf{e}_0, \tag{A7}$$

and

$$r_x=-\frac{1}{\sqrt{2}}(r_{+1}^{(1)}-r_{-1}^{(1)}),\quad r_y=\frac{i}{\sqrt{2}}(r_{+1}^{(1)}+r_{-1}^{(1)}),$$
$$r_z=r_0^{(1)}, \tag{A8}$$

Consequently, we have for the Cartesian basis

$$\mathbf{e}_p^*=\mathbf{e}_p,\quad \mathbf{e}_p\cdot\mathbf{e}_{p'}^*=\delta_{pp'}, \tag{A9}$$

and

$$(r^*)_p=[r_p]^*, \tag{A10}$$

where $p=x,y,z$. Therefore adopting the standard definitions, we are left with the conclusion of expressing an arbitrary vector $\mathbf{r}$ and its complex conjugate $\mathbf{r}^*$ in the spherical tensor basis as

$$\mathbf{r}=r_{+1}^{(1)}\mathbf{e}_{+1}^*+r_0^{(1)}\mathbf{e}_0^*+r_{-1}^{(1)}\mathbf{e}_{-1}^* \tag{A11}$$

and

$$\mathbf{r}^*=[r_{+1}^{(1)}]^*\mathbf{e}_{+1}+[r_0^{(1)}]^*\mathbf{e}_0+[r_{-1}^{(1)}]^*\mathbf{e}_{-1}. \tag{A12}$$

Hence we can express an orthonormal set of unit vectors $\boldsymbol{\epsilon}_j$ in a generalized notation as

$$\boldsymbol{\epsilon}_j=\sum_i(\boldsymbol{\epsilon}_j)_i\mathbf{e}_i^*,\quad \boldsymbol{\epsilon}_j^*=(\boldsymbol{\epsilon}_j)^*=\sum_i[(\boldsymbol{\epsilon}_j)_i]^*\mathbf{e}_i,$$
$$\boldsymbol{\epsilon}_i\cdot\boldsymbol{\epsilon}_j^*=\delta_{ij}, \tag{A13}$$

where the standard components of the unit vectors are defined as

$$(\boldsymbol{\epsilon}_j)_i=\boldsymbol{\epsilon}_j\cdot\mathbf{e}_i,\quad [(\boldsymbol{\epsilon}_j)_i]^*=\boldsymbol{\epsilon}_j^*\cdot\mathbf{e}_i^*,\quad (\boldsymbol{\epsilon}_j^*)_i=\boldsymbol{\epsilon}_j^*\cdot\mathbf{e}_i. \tag{A14}$$

Special care must be taken in interpreting Eq. (A14). We take $(\boldsymbol{\epsilon}_j)_i$ to represent the i component of the unit vector $\boldsymbol{\epsilon}_j$, $[(\boldsymbol{\epsilon}_j)_i]^*$ to represent the complex conjugate of the i component of the unit vector $\boldsymbol{\epsilon}_j$, and $(\boldsymbol{\epsilon}_j^*)_i$ to represent the i component of the complex conjugate of the unit vector $\boldsymbol{\epsilon}_j$, i.e., $\boldsymbol{\epsilon}_j^*$.

For light in a pure state of arbitrary polarization propagating along the space-fixed Z axis (such a choice is always possible), its polarization unit vector and its complex conjugate may be represented by

$$\begin{aligned}\boldsymbol{\epsilon}_j &= \cos\phi_j \mathbf{e}_x + e^{i\delta_j}\sin\phi_j \mathbf{e}_y \\ &= \frac{1}{\sqrt{2}}[\cos\phi_j - ie^{i\delta_j}\sin\phi_j]\mathbf{e}^*_{-1} \\ &\quad -\frac{1}{\sqrt{2}}[\cos\phi_j + ie^{i\delta_j}\sin\phi_j]\mathbf{e}^*_{+1} \end{aligned} \tag{A15}$$

and

$$\begin{aligned}\boldsymbol{\epsilon}^*_j &= \cos\phi_j \mathbf{e}_x + e^{-i\delta_j}\sin\phi_j \mathbf{e}_y \\ &= \frac{1}{\sqrt{2}}[\cos\phi_j - ie^{-i\delta_j}\sin\phi_j]\mathbf{e}^*_{-1} \\ &\quad -\frac{1}{\sqrt{2}}[\cos\phi_j + ie^{-i\delta_j}\sin\phi_j]\mathbf{e}^*_{+1}, \end{aligned} \tag{A16}$$

where ϕ_j ranges from 0 to π and δ_j is the phase necessary to describe elliptical polarization. Reference to Eqs. (A13)–(A16) shows that

$$\begin{aligned}&(\boldsymbol{\epsilon}_j)_x = \cos\phi_j, \quad (\boldsymbol{\epsilon}^*_j)_x = \cos\phi_j, \\ &(\boldsymbol{\epsilon}_j)_y = e^{i\delta_j}\sin\phi, \quad (\boldsymbol{\epsilon}^*_j)_y = e^{-i\delta_j}\sin\phi_j, \\ &(\boldsymbol{\epsilon}_j)^{(1)}_{+1} = -\frac{1}{\sqrt{2}}[\cos\phi_j + ie^{i\delta_j}\sin\phi_j], \\ &(\boldsymbol{\epsilon}^*_j)^{(1)}_{+1} = -\frac{1}{\sqrt{2}}[\cos\phi_j + ie^{-i\delta_j}\sin\phi_j], \\ &(\boldsymbol{\epsilon}_j)^{(1)}_{-1} = \frac{1}{\sqrt{2}}[\cos\phi_j - ie^{i\delta_j}\sin\phi_j], \\ &(\boldsymbol{\epsilon}^*_j)^{(1)}_{-1} = \frac{1}{\sqrt{2}}[\cos\phi_j - ie^{-i\delta_j}\sin\phi_j]. \end{aligned} \tag{A17}$$

For completeness we define left circularly polarized light[66] ($\phi_L = \pi/4$, $\delta_L = \pi/2$) as

$$\boldsymbol{\epsilon}_L = \frac{1}{\sqrt{2}}(\mathbf{e}_x + i\mathbf{e}_y) = \mathbf{e}^*_{-1}, \tag{A18}$$

right circularly polarized light ($\phi_R = 5\pi/4$, $\delta_R = -\pi/2$) as

$$\boldsymbol{\epsilon}_R = -\frac{1}{\sqrt{2}}(\mathbf{e}_x - i\mathbf{e}_y) = \mathbf{e}^*_{+1}, \tag{A19}$$

and light of arbitrary linear polarization ($\delta_j = 0$) as

$$\boldsymbol{\epsilon}_j = \cos\phi_j \mathbf{e}_x + \sin\phi_j \mathbf{e}_y = \frac{1}{\sqrt{2}}[e^{-i\phi_j}\mathbf{e}^*_{-1} - e^{i\phi_j}\mathbf{e}^*_{+1}]. \tag{A20}$$

The polarization tensors of Eq. (51) in the text are expanded and expressed in the spherical tensor basis as

$$\begin{aligned}&F(\boldsymbol{\epsilon}_4, \boldsymbol{\epsilon}_i, \boldsymbol{\epsilon}_j, \boldsymbol{\epsilon}_2; K) \\ &= \sum_{Q,q,q'} (-1)^Q (2K+1)(\boldsymbol{\epsilon}^*_4)^{(1)}_{-q}(\boldsymbol{\epsilon}_j)^{(1)}_{q+Q}(\boldsymbol{\epsilon}^*_2)^{(1)}_{-q'} \\ &\quad \times (\boldsymbol{\epsilon}_i)^{(1)}_{q'-Q}\begin{pmatrix} 1 & 1 & K \\ -q & q+Q & -Q \end{pmatrix} \\ &\quad \times \begin{pmatrix} 1 & 1 & K \\ -q' & q'-Q & Q \end{pmatrix}, \end{aligned} \tag{A21}$$

where the terms in parenthesis are 3-j symbols. The polarization tensors in the Cartesian basis are readily worked out using Eq. (A4) and (A21). The resulting expression does not have a compact form, so the polarization tensors are presented for each value of K, i.e.,

$$\begin{aligned}F(\boldsymbol{\epsilon}_4, \boldsymbol{\epsilon}_i, \boldsymbol{\epsilon}_j, \boldsymbol{\epsilon}_2; 0) &= \tfrac{1}{3}\{[(\boldsymbol{\epsilon}^*_4)_x(\boldsymbol{\epsilon}_j)_x + (\boldsymbol{\epsilon}^*_4)_y(\boldsymbol{\epsilon}_j)_y \\ &\quad + (\boldsymbol{\epsilon}^*_4)_z(\boldsymbol{\epsilon}_j)_z][(\boldsymbol{\epsilon}^*_2)_x(\boldsymbol{\epsilon}_i)_x + (\boldsymbol{\epsilon}^*_2)_y(\boldsymbol{\epsilon}_i)_y \\ &\quad + (\boldsymbol{\epsilon}^*_2)_z(\boldsymbol{\epsilon}_i)_z]\}, \end{aligned} \tag{A22a}$$

$$\begin{aligned}&F(\boldsymbol{\epsilon}_4, \boldsymbol{\epsilon}_i, \boldsymbol{\epsilon}_j, \boldsymbol{\epsilon}_2; 1) \\ &= -\frac{1}{2}\{[(\boldsymbol{\epsilon}^*_4)_x(\boldsymbol{\epsilon}_j)_y - (\boldsymbol{\epsilon}^*_4)_y(\boldsymbol{\epsilon}_j)_x][(\boldsymbol{\epsilon}^*_2)_x(\boldsymbol{\epsilon}_i)_y - (\boldsymbol{\epsilon}^*_2)_y \\ &\quad \times(\boldsymbol{\epsilon}_i)_x] + [(\boldsymbol{\epsilon}^*_4)_z(\boldsymbol{\epsilon}_j)_x - (\boldsymbol{\epsilon}^*_4)_x(\boldsymbol{\epsilon}_j)_z] \\ &\quad \times[(\boldsymbol{\epsilon}^*_2)_z(\boldsymbol{\epsilon}_i)_x - (\boldsymbol{\epsilon}^*_2)_x(\boldsymbol{\epsilon}_i)_z] + [(\boldsymbol{\epsilon}^*_4)_z(\boldsymbol{\epsilon}_j)_y \\ &\quad - (\boldsymbol{\epsilon}^*_4)_y(\boldsymbol{\epsilon}_j)_z][(\boldsymbol{\epsilon}^*_2)_z(\boldsymbol{\epsilon}_i)_y - (\boldsymbol{\epsilon}^*_2)_y(\boldsymbol{\epsilon}_i)_z]\}, \end{aligned} \tag{A22b}$$

and

$$\begin{aligned}F(\boldsymbol{\epsilon}_4, \boldsymbol{\epsilon}_i, \boldsymbol{\epsilon}_j, \boldsymbol{\epsilon}_2; 2) &= \tfrac{1}{6}\{[2(\boldsymbol{\epsilon}^*_4)_z(\boldsymbol{\epsilon}_j)_z - (\boldsymbol{\epsilon}^*_4)_x(\boldsymbol{\epsilon}_j)_x - (\boldsymbol{\epsilon}^*_4)_y(\boldsymbol{\epsilon}_j)_y][2(\boldsymbol{\epsilon}^*_2)_z(\boldsymbol{\epsilon}_i)_z - (\boldsymbol{\epsilon}^*_2)_x(\boldsymbol{\epsilon}_i)_x - (\boldsymbol{\epsilon}^*_2)_y(\boldsymbol{\epsilon}_i)_y]\} + \tfrac{1}{2}\{[(\boldsymbol{\epsilon}^*_4)_z(\boldsymbol{\epsilon}_j)_x \\ &\quad + (\boldsymbol{\epsilon}^*_4)_x(\boldsymbol{\epsilon}_j)_z][(\boldsymbol{\epsilon}^*_2)_z(\boldsymbol{\epsilon}_i)_x + (\boldsymbol{\epsilon}^*_2)_x(\boldsymbol{\epsilon}_i)_z] + [(\boldsymbol{\epsilon}^*_4)_z(\boldsymbol{\epsilon}_j)_y + (\boldsymbol{\epsilon}^*_4)_y(\boldsymbol{\epsilon}_j)_z][(\boldsymbol{\epsilon}^*_2)_z(\boldsymbol{\epsilon}_i)_y + (\boldsymbol{\epsilon}^*_2)_y(\boldsymbol{\epsilon}_i)_z] \\ &\quad + [(\boldsymbol{\epsilon}^*_4)_x(\boldsymbol{\epsilon}_j)_x - (\boldsymbol{\epsilon}^*_4)_y(\boldsymbol{\epsilon}_j)_y][(\boldsymbol{\epsilon}^*_2)_x(\boldsymbol{\epsilon}_i)_x - (\boldsymbol{\epsilon}^*_2)_y(\boldsymbol{\epsilon}_i)_y] + [(\boldsymbol{\epsilon}^*_4)_x(\boldsymbol{\epsilon}_j)_y + (\boldsymbol{\epsilon}^*_4)_y(\boldsymbol{\epsilon}_j)_x] \\ &\quad \times[(\boldsymbol{\epsilon}^*_2)_x(\boldsymbol{\epsilon}_i)_y + (\boldsymbol{\epsilon}^*_2)_y(\boldsymbol{\epsilon}_i)_x]\}. \end{aligned} \tag{A22c}$$

Equations (A21) and (A22) can be used to obtain the DFWM signal intensity along $\boldsymbol{\epsilon}_4$, i.e., the DFWM signal direction. It is often possible to predict the direction of $\boldsymbol{\epsilon}_4$ by invoking symmetry arguments of $\chi^{(3)}$.[62] These equations also apply for polarized detection in which case $\boldsymbol{\epsilon}_4$ is the polarization axis of the DFWM detector.

For experiments in which it is difficult to predict the DFWM signal direction by symmetry arguments or for unpolarized detection, it is more useful to express the DFWM signal intensity in terms of its components. Rewriting the DFWM signal intensity of Eq. (19) in Sec III A in terms of the components of the generalized basis of orthonormal unit vectors defined by Eqs. (A13) and (A14) yields

$$I_{\mathrm{DFWM}} \propto \langle |\mathbf{P}^{(3)}(\mathbf{r},t)|^2 \rangle = \frac{1}{2} \sum_j |\mathscr{P}_j^{(3)}|^2 \tag{A23}$$

where $\mathscr{P}_j^{(3)}$ is the scalar amplitude of the j component of $\mathbf{P}^{(3)}(\mathbf{r},t)$ and is defined as

$$\mathscr{P}_j^{(3)} = \mathbf{P}_{\mathrm{DFWM}}^{(3)} \cdot \boldsymbol{\epsilon}_j^* . \tag{A24}$$

Equation (A24) can be rewritten using the notation of Eqs. (45)–(51) as

$$\mathscr{P}_j^{(3)} = \frac{9\epsilon_0^2\hbar}{8\pi^2}\left[N_g - \frac{(2J_g+1)}{(2J_e+1)}N_e\right][B_{ge}(J_g,J_e)]^2 \mathscr{E}_1\mathscr{E}_2^*\mathscr{E}_3\left\{\sum_K L_{12}^g(\omega,K)G(J_g,J_e;K)F(\boldsymbol{\epsilon}_j,\boldsymbol{\epsilon}_1,\boldsymbol{\epsilon}_3,\boldsymbol{\epsilon}_2;K)\right.$$
$$+\sum_K L_{12}^e(\omega,K)G(J_e,J_g;K)F(\boldsymbol{\epsilon}_j,\boldsymbol{\epsilon}_1,\boldsymbol{\epsilon}_3,\boldsymbol{\epsilon}_2;K)+\sum_K L_{32}^g(\omega,K)G(J_g,J_e;K)F(\boldsymbol{\epsilon}_j,\boldsymbol{\epsilon}_3,\boldsymbol{\epsilon}_1,\boldsymbol{\epsilon}_2;K)$$
$$\left.+\sum_K L_{32}^e(\omega,K)G(J_e,J_g;K)F(\boldsymbol{\epsilon}_j,\boldsymbol{\epsilon}_3,\boldsymbol{\epsilon}_1,\boldsymbol{\epsilon}_2;K)\right\}, \tag{A25}$$

where all of the terms have their previous meanings.

Equation (A25) can also be expressed in terms of its standard components. In the spherical tensor basis $\boldsymbol{\epsilon}_j = \mathbf{e}_q^*$, and the polarization tensors in Eq. (A25) take on the form

$$F(\mathbf{e}_q^*,\boldsymbol{\epsilon}_i,\boldsymbol{\epsilon}_j,\boldsymbol{\epsilon}_2;K) = \sum_{Q=-K}^{K}(-1)^Q[e_q^{(1)}\otimes\boldsymbol{\epsilon}_j^{(1)}]_Q^{(K)}[\boldsymbol{\epsilon}_2^{*(1)}\otimes\boldsymbol{\epsilon}_i^{(1)}]_{-Q}^{(K)}. \tag{A26}$$

Substitution of $(e_q)_{-q''}^{(1)} = \mathbf{e}_q \cdot \mathbf{e}_{-q''} = (-1)^q\delta_{qq''}$ into Eq. (A21) gives

$$F(\mathbf{e}_q^*,\boldsymbol{\epsilon}_i,\boldsymbol{\epsilon}_j,\boldsymbol{\epsilon}_2;K) = \sum_{Q,q'}(-1)^{q+Q}(2K+1)(\boldsymbol{\epsilon}_j)_{q+Q}^{(1)}(\boldsymbol{\epsilon}_2^*)_{-q'}^{(1)}(\boldsymbol{\epsilon}_i)_{q'-Q}^{(1)}$$
$$\times\begin{pmatrix}1 & 1 & K\\ -q & q+Q & -Q\end{pmatrix}\begin{pmatrix}1 & 1 & K\\ -q' & q'-Q & Q\end{pmatrix} \tag{A27}$$

which can be used in Eq. (A25) to generate the expression for the scalar amplitude of the q component of the nonlinear polarization $\mathbf{P}^{(3)}(\mathbf{r},t)$. The resulting expression is equivalent to Eqs. (33) and (34) of Ref. 30 derived using a density matrix approach in the weak-field limit. In the Cartesian basis $\boldsymbol{\epsilon}_j = \mathbf{e}_p^*$, and substitution of $(\boldsymbol{\epsilon}_p)_{p''} = \mathbf{e}_p\cdot\mathbf{e}_{p''} = \delta_{pp''}$ into Eq. (A22) for $p = y$ gives the Y component of the polarization tensors as a function of K, namely,

$$F(\mathbf{e}_y^*,\boldsymbol{\epsilon}_i,\boldsymbol{\epsilon}_j,\boldsymbol{\epsilon}_2;0) = \tfrac{1}{3}\{[(\boldsymbol{\epsilon}_j)_y(\boldsymbol{\epsilon}_2^*)_x(\boldsymbol{\epsilon}_i)_x+(\boldsymbol{\epsilon}_j)_y(\boldsymbol{\epsilon}_2^*)_y(\boldsymbol{\epsilon}_i)_y + (\boldsymbol{\epsilon}_j)_y(\boldsymbol{\epsilon}_2^*)_z(\boldsymbol{\epsilon}_i)_z]\}, \tag{A28a}$$

$$F(\mathbf{e}_y^*,\boldsymbol{\epsilon}_i,\boldsymbol{\epsilon}_j,\boldsymbol{\epsilon}_2;1) = \tfrac{1}{2}\{[(\boldsymbol{\epsilon}_j)_x(\boldsymbol{\epsilon}_2^*)_x(\boldsymbol{\epsilon}_i)_y-(\boldsymbol{\epsilon}_j)_x(\boldsymbol{\epsilon}_2^*)_y(\boldsymbol{\epsilon}_i)_x] + [(\boldsymbol{\epsilon}_j)_z(\boldsymbol{\epsilon}_2^*)_z(\boldsymbol{\epsilon}_i)_y-(\boldsymbol{\epsilon}_j)_z(\boldsymbol{\epsilon}_2^*)_y(\boldsymbol{\epsilon}_i)_z]\}, \tag{A28b}$$

and

$$F(\mathbf{e}_y^*,\boldsymbol{\epsilon}_i,\boldsymbol{\epsilon}_j,\boldsymbol{\epsilon}_2;2) = -\tfrac{1}{6}\{[2(\boldsymbol{\epsilon}_j)_y(\boldsymbol{\epsilon}_2^*)_z(\boldsymbol{\epsilon}_i)_z-(\boldsymbol{\epsilon}_j)_y(\boldsymbol{\epsilon}_2^*)_x(\boldsymbol{\epsilon}_i)_x-(\boldsymbol{\epsilon}_j)_y(\boldsymbol{\epsilon}_2^*)_y \times(\boldsymbol{\epsilon}_i)_y]\}+\tfrac{1}{2}\{[(\boldsymbol{\epsilon}_j)_z(\boldsymbol{\epsilon}_2^*)_z(\boldsymbol{\epsilon}_i)_y+(\boldsymbol{\epsilon}_j)_z(\boldsymbol{\epsilon}_2^*)_y(\boldsymbol{\epsilon}_i)_z] -[(\boldsymbol{\epsilon}_j)_y(\boldsymbol{\epsilon}_2^*)_x(\boldsymbol{\epsilon}_i)_x-(\boldsymbol{\epsilon}_j)_y(\boldsymbol{\epsilon}_2^*)_y(\boldsymbol{\epsilon}_i)_y]+[(\boldsymbol{\epsilon}_j)_x \times(\boldsymbol{\epsilon}_2^*)_x(\boldsymbol{\epsilon}_i)_y+(\boldsymbol{\epsilon}_j)_x(\boldsymbol{\epsilon}_2^*)_y(\boldsymbol{\epsilon}_i)_x]\}. \tag{A28c}$$

The X and Z components are readily evaluated by reiterating the procedure for $p = x$ and z, respectively.

For the near collinear phase matching geometries and pure polarization states described in this paper, only one standard component is nonzero. This result can be verified by substituting the polarizations of the input fields $\mathbf{E}_1$, $\mathbf{E}_2$, and $\mathbf{E}_3$ into Eqs. (A27) and (A28) using the definitions of Eqs. (A18) and (A19) for circularly polarized light and Eq. (A20) for $\phi_j = 0$ and $\phi_j = \pi/2$ linearly polarized light. These substitutions yield the results presented in Table V. For noncollinear phase matching geometries, mixed polarization states, or both, all of the components must be determined.

The above expressions refer to the standard components of the electric fields when all the fields are defined with respect to a common reference frame. For example, in the case of noncollinear phase matching geometries, all the fields must be rotated into a common frame of reference (we suggest the detection frame) before the standard components can be determined. Such frame rotations are readily carried out in the spherical tensor basis using Wigner rotation matrices or in the Cartesian basis using direction cosine matrices. For more information on this topic, see Ref. 3, Chap. 3.

[1] D. A. Case, G. M. McClelland, and D. R. Herschbach, *Mol. Phys.* **35**, 541 (1978).
[2] C. H. Greene and R. N. Zare, J. Chem. Phys. **78**, 6741 (1983).
[3] R. N. Zare, *Angular Momentum* (Wiley, New York, 1988).
[4] D. R. Crosley, Opt. Eng. **20**, 511 (1981).
[5] A. C. Eckbreth, *Laser Diagnostics for Combustion Temperature and Species* (Abacus, Cambridge, MA, 1988).
[6] K. J. Rensberger, J. B. Jeffries, R. A. Copeland, K. Kohse-Höinghaus, M. L. Wise and D. R. Crosley, Appl. Opt. **28**, 3556 (1989).
[7] R. P. Lucht and N. M. Laurendeau, Appl. Opt. **18**, 856 (1979); R. P. Lucht,

D. W. Sweeney, and N. M. Laurendeau, *ibid.* **19**, 3295 (1980).
[8] R. Altkorn and R. N. Zare, Annu. Rev. Phys. Chem. **35**, 265 (1984).
[9] N. Billy, B. Girard, G. Gouedard, and J. Vigué, Mol. Phys. **61**, 65 (1987).
[10] R. L. Abrams, J. F. Lam, R. C. Lind, D. G. Steel, and P. F. Liao, in *Optical Phase Conjugation*, edited by R. A. Fisher (Academic, New York, 1983), Chap. 8.
[11] R. L. Farrow and D. J. Rakestraw, Science **257**, 1894 (1992).
[12] R. L. Abrams and R. C. Lind, Opt. Lett. **2**, 94 (1978); **3**, 205(E) (1978).
[13] R. L. Farrow, D. J. Rakestraw, and T. Dreier, J. Opt. Soc. Am. B **9**, 1770 (1992); T. Dreier and D. J. Rakestraw, Appl. Phys. B **50**, 479 (1990); T. Dreier and D. J. Rakestraw, Opt. Lett. **15**, 72 (1990).
[14] M. Winter and P. P. Radi, Opt. Lett. **17**, 320 (1992).
[15] B. Yip, P. M. Danehy and R. K. Hanson, Opt. Lett. **17**, 751 (1992).
[16] S. Williams, D. S. Green, S. Sethuraman, and R. N. Zare, J. Am. Chem. Soc. **114**, 9122 (1992); T. G. Owano, C. H. Kruger, D. S. Green, S. Williams, and R. N. Zare, Diamond Relat. Mat. **2**, 661 (1993); D. S. Green, T. G. Owano, S. Williams, D. G. Goodwin, R. N. Zare, and C. H. Kruger, Science **259**, 1726 (1993).
[17] S. Williams, R. N. Zare, and L. A. Rahn, J. Chem. Phys. **101**, 1093 (1994).
[18] D. R. Meacher, A. Charlton, P. Ewart, J. Cooper, and G. Alber, Phys. Rev. A **42**, 3018 (1990); J. Cooper, A. Charlton, D. R. Meacher, P. Ewart, and G. Alber, *ibid.* **40**, 5705 (1989); G. Alber, J. Cooper, and P. Ewart, *ibid.* **31**, 2344 (1985).
[19] D. Bloch and M. Ducloy, J. Opt. Soc. Am. **73**, 635 (1983); **73**, 1844(E) (1983).
[20] G. G. Adonts and D. G. Akopyan, J. Phys. B **18**, 3407 (1985).
[21] M. Ducloy, F. A. M. de Oliveira, and D. Bloch, Phys. Rev. A **32**, 1614 (1985).
[22] S. Le Boiteux, P. Simoneau, D. Bloch, F. A. M. de Oliveira, and M. Ducloy, IEEE J. Quantum Electron. **QE-22**, 1229 (1986).
[23] G. P. Agrawal, Opt. Lett. **8**, 359 (1983).
[24] G. Grynberg, M. Pinard, and P. Verkerk, Opt. Commun. **50**, 261 (1984).
[25] M. Pinard, B. Kleinmann, and G. Grynberg, Opt. Commun. **51**, 281 (1984).
[26] G. Grynberg, M. Pinard, and P. Verkerk, J. Phys. (Paris) **47**, 617 (1986).
[27] P. Verkerk, M. Pinard, and G. Grynberg, Phys. Rev. A **35** (1987).
[28] R. P. Lucht, R.L. Farrow, and D. J. Rakestraw, J. Opt. Soc. Am. B **10**, 1508 (1993).
[29] J. F. Lam and R. L. Abrams, Phys. Rev. A **26**, 1539 (1982).
[30] M. Ducloy and D. Bloch, Phys. Rev. A **30**, 3107 (1984).
[31] P. R. Berman, D. G. Steel, G. Khitrova, and J. Liu, Phys. Rev. A **38**, 252 (1988).
[32] F. Aguillion, IEEE J. Quantum Electron. **QE-25**, 1947 (1989).
[33] B. Attal-Trétout, P. Monot, and K. Müller-Dethlefs, Mol. Phys. **73**, 1257 (1991); B. Attal-Trétout and K. Müller-Dethlefs, Ber. Bunsenges. Phys. Chem. **89**, 318 (1985).
[34] A. A. Panteleev, Sov. Phys. JETP **72**, 939 (1991).
[35] A. I. Alekseev, Sov. Phys. JETP **74**, 227 (1992).
[36] I. Aben, W. Ubachs, G. van der Zwan, and W. Hogervorst, Chem. Phys. **169**, 113 (1993).
[37] H. Bervas, S. Le Boiteux, L. Labrunie, and B. Attal-Trétout, Mol. Phys. **79**, 911 (1993).
[38] D. Kupiszewska and B. J. Whitaker, J. Chem. Soc. Faraday Trans. **89**, 2951 (1993).
[39] E. Freidman-Hill, L. A. Rahn, and R. L. Farrow, J. Chem. Phys. (in press).
[40] S. A. J. Druet and J.-P. E. Taran, Prog. Quantum Electron. **7**, 1 (1981).
[41] Y. Prior, IEEE J. Quantum Electron. **QE-20**, 37 (1984).
[42] R. C. Hilborn, Am. J. Phys. **50**, 982 (1982).
[43] M. Ducloy and D. Bloch, J. Phys. (Paris) **42**, 711 (1981).
[44] H. J. Eichler, P. Günter and D. W. Pohl, *Laser-Induced Dynamic Gratings* (Springer, Berlin, 1986).
[45] In laser-induced grating phenomena molecular diffusion will fill the grating nulls and will deplete the peaks, i.e., cause wash out. In general the entire molecular velocity distribution along the grating k-vector contributes. This effect is discussed in T. S. Rose, W. L. Wilson, G. Wäckerle, and M. D. Fayer, J. Chem. Phys. **86**, 5370 (1987). In DFWM, however, the counterpropagating pump fields insure that only the sub-Doppler projection of the molecular velocity distribution on the grating k-vector contributes. Because both the grating spacing and the velocity projection increase as $1/\sin(\theta/2)$, the large- and small-spaced gratings wash out to the same degree in the infinite Doppler limit. If the Doppler width is finite, however, the projection along the large-spaced grating's k vector is finite, and it will be washed out to a lesser degree.
[46] L. A. Rahn and M. S. Brown, Opt. Lett. (in press).
[47] J. W. Tester, H. R. Holgate, F. J. Armellini, P. A. Webley, W. R. Killilea, G. T. Hong, and H. E. Barner, in *Emerging Technologies in Hazardous Waste Management III*, edited by D. W. Tedder and F. G. Pohland (American Chemical Society, Washington D.C., 1993), Chap. 3.
[48] S. M. Wandzura, Opt. Lett. **4**, 208 (1979).
[49] P. H. Paul, R. L. Farrow, and P. M. Danahy, in preparation.
[50] S. Williams, L. A. Rahn, P. H. Paul, J. W. Forsman, and R. N. Zare, Opt. Lett. (submitted).
[51] D. E. Govoni, J. A. Booze, A. Sinha, and F. F. Crim, Chem. Phys. Lett. **216**, 525 (1994).
[52] J. T. Fourkas, R. Trebino, and M. D. Fayer, J. Chem. Phys. **97**, 69 (1992).
[53] J. T. Fourkas, R. Trebino, and M. D. Fayer, J. Chem. Phys. **97**, 78 (1992).
[54] J. Nunes, W. G. Tong, L. A. Rahn, and D. W. Chandler (in preparation).
[55] U. Fano and J. H. Macek, Rev. Mod. Phys. **45**, 553 (1973).
[56] A. Omont, Prog. Quantum Electron. **5**, 69 (1977).
[57] K. Blum, *Density Matrix Theory and Applications* (Plenum, New York, 1981).
[58] T. K. Yee and T. K. Gustafson, Phys. Rev. A **18**, 1597 (1978).
[59] R. Trebino, Phys. Rev. A **38**, 2921 (1988).
[60] U. Fano and G. Racah, *Irreducible Tensorial Sets* (Academic, New York, 1959).
[61] B. R. Judd, *Angular Momentum Theory for Diatomic Molecules* (Academic, New York, 1975).
[62] P. N. Butcher and D. Cotter, *The Elements of Nonlinear Optics* (Cambridge University, Cambridge, 1990). We use the numerical definitions and convention established by these authors; however, our analysis uses double-sided Feynman diagrams whereas these authors use single-sided diagrams which can lead to errors.
[63] A good discussion of isotropic relaxation and broadening of optical transitons is given in Ref. 56, pp. 108–113.
[64] Because $\mathcal{E}_4=(ik_4L/2\epsilon_0)\mathcal{P}_4^{(3)}$ there is an additional L^2 dependence where L is the interaction length of the fields in the medium. See Ref. 30, Eq. (23) and Ref. 62, pp. 217–218.
[65] S. Williams, R. N. Zare and L. A. Rahn (in preparation).
[66] E. Hecht, *Optics* (Addison-Wesley, Reading, 1987), pp. 270–273.